

**STUDY OF POLYVINYL ALCOHOL (PVOH) ADDED WITH
CALCINED CUTTLEBONE AND MONTMORILLONITE (MMT)**

THUM JIA-YI


**A project report submitted in partial fulfilment of the
requirements for the award of Bachelor of Engineering
(Honours) Chemical Engineering**

**Lee Kong Chian Faculty of Engineering and Science
Universiti Tunku Abdul Rahman**

April 2020

DECLARATION

I hereby declare that this project report is based on my original work except for citations and quotations which have been duly acknowledged. I also declare that it has not been previously and concurrently submitted for any other degree or award at UTAR or other institutions.

Signature : 

Name : Thum Jia-Yi

ID No. : 1504107

Date : 30th March 2020

APPROVAL FOR SUBMISSION

I certify that this project report entitled “**STUDY OF POLYVINYL ALCOHOL (PVOH) ADDED WITH CALCINED CUTTLEBONE AND MONTMORILLONITE (MMT)**” was prepared by **THUM JIA-YI** has met the required standard for submission in partial fulfilment of the requirements for the award of Bachelor of Engineering (Honours) Chemical Engineering at Universiti Tunku Abdul Rahman.

Approved by,

Signature

:



Supervisor

:

Ir. Dr. Lee Tin Sin

Date

:

15/05/2020

The copyright of this report belongs to the author under the terms of the copyright Act 1987 as qualified by Intellectual Property Policy of Universiti Tunku Abdul Rahman. Due acknowledgement shall always be made of the use of any material contained in, or derived from, this report.

© 2020, Thum Jia-Yi. All right reserved.

ACKNOWLEDGEMENTS

I would like to thank everyone who had contributed to the successful completion of this project. I would like to express my gratitude to my research supervisor, Ir. Dr. Lee Tin Sin for his invaluable advice, guidance and his enormous patience throughout the development of the research.

In addition, I would also like to express my gratitude to my loving parents and friends who had helped and given me encouragement as my research was conducted.

ABSTRACT

This study aims to investigate the effects on calcined cuttlebone reinforced polyvinyl alcohol (PVOH)/ montmorillonite (MMT) blends. Generally, polyvinyl alcohol-cuttlebone-montmorillonite (PVOH-cuttlebone-MMT) nanocomposites were prepared using solution casting method. Calcined cuttlebone particles were added to the PVOH matrix at different amount of 2 and 5 phr with fixed MMT ranging from 1 to 3 phr. The results showed the tensile strength of cuttlebone added PVOH-MMT composites at fixed 1 phr MMT was observed marginally lower when the cuttlebone increased from 2 phr to 5 phr due to the poor distribution of agglomerated particles. Nevertheless, at higher fixed loading level of MMT, it was found that the addition of cuttlebone at high amount (5 phr) exhibited reinforcing effect in PVOH/ MMT blends. This also found to be consistent with the scanning electron microscopy observation where the dispersion of higher amount of cuttlebone in PVOH-MMT blends was noted to be more homogeneous than lower amount of cuttlebone. Besides, based on the X-ray diffraction analysis, the addition of cuttlebone has significantly enhanced the intercalation of effect of MMT particles in PVOH matrix. Furthermore, the infrared number of hydroxyl group for all composites reduced gradually with the increasing amount of cuttlebone. The addition of cuttlebone has shown the “red shift” effect indicating the formation of hydrogen bonding induced by cuttlebone. Lastly, lower enthalpy of melting was detected in relation to higher loading level of cuttlebone embedded in PVOH-MMT blends. In conclusion, the blending of cuttlebone in PVOH-MMT are favourable to obtain better properties of composites.

TABLE OF CONTENTS

DECLARATION		i
APPROVAL FOR SUBMISSION		ii
ACKNOWLEDGEMENTS		iv
ABSTRACT		v
TABLE OF CONTENTS		vi
LIST OF TABLES		ix
LIST OF FIGURES		x
LIST OF SYMBOLS / ABBREVIATIONS		xiii
 CHAPTER		
1	INTRODUCTION	14
1.1	Background	14
1.2	Problem Statements	15
1.3	Objectives	16
1.4	Scope of Study	16
2	LITERATURE REVIEW	18
2.1	Polyvinyl Alcohol (PVOH)	18
2.1.1	Chemical structure of PVOH	18
2.1.2	Properties of PVOH	19
2.1.3	Application of PVOH	20
2.1.4	Morphologies of PVOH	20
2.1.5	PVOH in Polymer Nanocomposite	20
2.2	Montmorillonite (MMT)	21
2.2.1	Chemical Structure of MMT	21
2.2.2	Properties of MMT	23
2.2.3	Application of MMT	23
2.2.4	Comparison between MMT with Other Silicates	24
2.2.5	MMT in Polymer nanocomposite	24
2.3	Cuttlebone	25
2.3.1	Chitosan	26
2.3.2	Hydroxyapatite (HAP)	26

2.4	PVOH-MMT nanocomposites	28
2.4.1	Tensile Test	29
2.4.2	SEM	30
2.4.3	XRD	31
2.4.4	FTIR	33
2.4.5	TGA	34
2.4.6	DSC	35
2.5	Natural Rubber-Cuttlebone Composites	36
2.6	Epoxy-Cuttlebone Composites	38
2.7	PVOH-HAP COMPOSITES	44
3	MATERIALS AND METHODOLOGY	46
3.1	Materials	46
3.2	Formulation	46
3.3	Sample Preparation	47
3.4	Characterisation Test	47
3.4.1	Tensile Test	47
3.4.2	Scanning Electron Microscopy (SEM) Observation	47
3.4.3	X-ray Diffraction (XRD) Test	48
3.4.4	Fourier Transform Infrared Spectrometry (FTIR) Test	48
3.4.5	Differential Scanning Calorimetry (DSC) Test	48
4	RESULTS AND DISCUSSIONS	49
4.1	Mechanical Properties Analysis	49
4.1.1	Tensile Strength Test	49
4.1.2	Young's Modulus	51
4.1.3	Tensile Elongation	52
4.2	Scanning Electron Microscopy (SEM)	53
4.2.1	Interaction of PVOH-Calcined Cuttlebone with Various Amount of MMT	53
4.2.2	Interaction of PVOH-MMT with Various Amount of Calcined Cuttlebone	57
4.3	X-Ray Diffraction (XRD) Test	58

4.3.1	Description of Peaks	58
4.3.2	Crystallite size and d-spacing of All PVOH - Cuttlebone - MMT Composites	60
4.3.3	Crystallinity	61
4.4	Fourier Transform Infrared (FTIR) Test	63
4.4.1	FTIR for All PVOH-Cuttlebone- MMT Nanocomposites	63
4.5	Differential Scanning Calorimetry (DSC) Test	68
4.5.1	Melting Temperature	68
4.5.2	Enthalpy of Melting	70
5	CONCLUSION AND RECCOMENDATION	73
5.1	Conclusion	73
5.2	Recommendation for Future Work	75
	REFERENCES	76

LIST OF TABLES

Table 2.1:	Summary of PVOH (Muhammad and Zulfiqar Ali, 2018).	18
Table 2.2:	Summary Descriptions of MMT (Gutierrez, 2018).	21
Table 2.3:	Inter-chain Separation and d-spacing of Neat PVOH and PVOH-MMT blends on Peak B (Bee et al., 2014).	33
Table 2.4:	Crystallinity Degree and Melting Temperature of PVOH and PVOH-MMT Composite (Allison et al., 2015).	34
Table 2.5:	Properties of Cross-linked Natural Rubber Filled with Cuttlebone Particles (Poompradub et al., 2008).	37
Table 2.6:	Maximum Temperature (T_{max}) and Glass transition Temperature (T_g) of Neat Epoxy and Epoxy-calcined cuttlebone Composite (Periasamy and Kumar, 2019).	41
Table 3.1:	Formulation of PVOH, MMT and Cuttlebone.	46
Table 4.1:	d-Spacing and Crystallite Size at $2\theta = 19.4^\circ$ for All PVOH-Cuttlebone-MMT Composites.	61
Table 4.2:	Wavenumbers of its Stretching Type for All PVOH-Calcined Cuttlebone-MMT Nanocomposites.	66
Table 4.3:	Melting Temperature, Onset and End Temperature of PVOH-Cuttlebone-MMT Nanocomposites.	72

LIST OF FIGURES

Figure 2.1:	The Crystalline Structure of MMT (Gutierrez, 2018).	22
Figure 2.2:	Types of composite structures (Ling, 2015).	25
Figure 2.3:	Cuttlebone's Section and the Scanning Electron Microscopy of Dorsal Field and Lamellar Matrix (Birchall and Thomas, 1983).	25
Figure 2.4:	Diffraction pattern of apatite structure with different calcination temperature treatments (green (800 °C), blue (900 °C), red (1000 °C)) (Henggu, Ibrahim and Suptijah, 2019).	28
Figure 2.5:	Intercalation and Exfoliation of Na ⁺ MMT on PVOH (Ooi, 2017).	29
Figure 2.6:	Mechanical Properties of Developed Nanocomposites with Various Amount of MMT in term of Young Modulus (Allison et al., 2015).	29
Figure 2.7:	Mechanical Properties of Developed Nanocomposites with Various amount of MMT in term of Elongation Value (Allison et al., 2015).	30
Figure 2.8:	Surface morphologies of fractured surface for (a) Neat PVOH (× 10 000), (b) Neat PVOH (× 30 000), (c) PVOH composites with added 0.5 phr MMT (×10 000), (d) PVOH composites with added 1.5 phr MMT (× 10 000), (e) PVOH composites with added 4.5 phr MMT (×10 000) (Bee et al., 2014).	31
Figure 2.9:	XRD Curves ($0^\circ \leq 2\theta \leq 3^\circ$) for PVOH with Different Loading Level of MMT (Bee et al., 2014).	32
Figure 2.10:	FTIR Spectrums of PVOH, MMT and PVOH- MMT Blends (Gaidukov, Danilenko and Gaidukova, 2015).	34
Figure 2.11:	Decomposition Rate of the Material as a Function of Clay Volume Fraction (Allison et al., 2015).	35
Figure 2.12:	DSC curves of pure PVOH and PVOH- MMT nanocomposites (Allison et al., 2015).	36

- Figure 2.13: SEM Image of Cross-linked Natural Rubber Filled with 5 phr, 40 phr and 100 phr Cuttlebone Particles Filler (Darder, Colilla and Ruiz-Hitzky, 2003). 38
- Figure 2.14: (a) Ultimate Tensile Strength, (b) Young Modulus, and (c) Elongation Percentage at Break of Cuttlebone in Different Particle Size Reinforced Epoxy Composites (Kamalbabu and Mohan Kumar, 2014). 39
- Figure 2.15: SEM micrograph of Neat Epoxy (Left) and cuttlebone in <75 μm particle size in reinforced composites (Right) (Kamalbabu and Mohan Kumar, 2014). 40
- Figure 2.16: Thermal Degradation (TG), Differential Thermogravimetry (DTG) and Differential Thermal Analysis (DTA) Curves of Cuttlebone Particles (Periasamy and Kumar, 2019). 40
- Figure 2.17: TGA Curve for Epoxy (EP), Epoxy-raw cuttlebone (EP/ CB) Composites, Epoxy-calcined cuttlebone (EP/HB) Composites, and Epoxy-commercial calcium carbonate (EP/ CC) composites (Periasamy and Kumar, 2019). 41
- Figure 2.18: DSC Curve for Epoxy (EP), Epoxy-raw cuttlebone (EP/CB) Composites, Epoxy-calcined cuttlebone (EP/HB) Composites, and Epoxy-commercial calcium carbonate (EP/CC) composites (Periasamy and Kumar, 2019). 42
- Figure 2.19: FTIR spectra of (a) Raw Cuttlebone, (b) Cuttlebone heated at 100 $^{\circ}\text{C}$; (c) Cuttlebone Heated at 400 $^{\circ}\text{C}$ and (d) Commercial CaCO_3 (Periasamy and Mohankumar, 2016). 43
- Figure 2.20: FTIR spectra of Sepia Cuttlebone at 900 $^{\circ}\text{C}$ (Florek et al., 2009). 43
- Figure 2.21: FTIR Spectra of Pure PVOH and PVOH-HAP Composites (Balgova et al., 2013). 45
- Figure 2.22: FTIR Spectrum of Pure HAP (Balgova et al, 2013). 45
- Figure 3.1: Stages of Preparation of Cuttlebone Particles. 46
- Figure 4.1: (a) Tensile Strength, (b) Young's Modulus and (c) Tensile Elongation (%) for PVOH-cuttlebone-MMT Nanocomposites. 50

Figure 4.2:	SEM of 2 phr Calcined Cuttlebone Incorporated into PVOH Matrix Added with (a) 1 phr MMT (b) 2 phr MMT and (c) 3 phr MMT.	55
Figure 4.3:	SEM of 5 phr Calcined Cuttlebone Incorporated into PVOH Matrix Added with (a) 1 phr MMT (b) 2 phr MMT and (c) 3 phr MMT.	56
Figure 4.4:	XRD Curves ($5^\circ \leq 2\theta \leq 40^\circ$) for (a) Pure Cuttlebone and PVOH Added with 2 phr of Pure Cuttlebone and Various Loading Level of MMT (b) Pure Cuttlebone and PVOH Added with 5 phr of Pure Cuttlebone and Various Loading Level of MMT.	59
Figure 4.5:	Crystallinity of All PVOH-Cuttlebone-MMT Composites.	62
Figure 4.6:	Infrared Spectrum of all PVOH-MMT Nanocomposites Added with 2 phr of Calcined Cuttlebone.	64
Figure 4.7:	Infrared Spectrum of all PVOH-MMT Nanocomposites Added with 5 phr Calcined Cuttlebone.	65
Figure 4.8	DSC Thermogram of PVOH-Cuttlebone-MMT Composites.	68
Figure 4.9:	Effect of Increasing MMT and Cuttlebone Loading Level on Melting Temperature.	69
Figure 4.10:	Effect of Increasing MMT and Cuttlebone Loading Level on Enthalpy of Melting.	71

LIST OF SYMBOLS / ABBREVIATIONS

mL	millilitre
mm	millimetre
mA	milli Ampere
kV	kilovolt
d	d-spacing
L	Crystallite size
λ	1.542 Å
K	Scherrer constant
θ	Bragg angle, radians
phr	Part per hundred resin
rpm	Revolutions per minute
T _g	Glass transition temperature, °C
T _m	Melting temperature, °C
CaO	Calcium oxide
CaCO ₃	Calcium carbonate
CO ₂	Carbon dioxide
EP	Epoxy
EP/CB	Epoxy-raw cuttlebone
EP/HB	Epoxy-calcined cuttlebone
EP/CC	Epoxy-calcium carbonate
HAP/HA	Hydroxyapatite
MMT	Montmorillonite
PVOH/ PVA	Polyvinyl alcohol
DSC	Differential scanning calorimetry
FTIR	Fourier transform infrared
SEM	Scanning electron microscopy
XRD	X-ray diffraction
TGA	Thermogravimetric analysis

CHAPTER 1

INTRODUCTION

1.1 Background

Nowadays, most of the plastic materials used are generally from petroleum-based products. These polymers are not resistant to degradation and eventually accumulated in the form of wastes. Hence, biodegradable polymers get the attention of researchers over past decades. Many studies have been carried out to develop the environmentally friendly materials (Qiu and Netravali, 2015). Biodegradable polymer, which is known as biopolymer can be decomposed in the presence of enzyme or microorganisms under aerobic or anaerobic condition. Biopolymer possesses high versatility, biodegradability and is also diverse in application, especially in biomedical field (Ashwin, Karthick and Arumugam, 2011).

Polyvinyl alcohol (PVOH) is one example of the biodegradable thermoplastic polymer. PVOH is produced from polyvinyl acetate through hydrolysis in the presence of hydroxyl groups on the carbon atom. PVOH polymer has characteristics of high water solubility and biocompatibility. It is also non-toxic and odourless. PVOH can form highly orientated crystal structure (Ling, 2015). PVOH is commonly applied in textile sizing, paper coating and food packaging. However, PVOH has disadvantages of insufficient strength and low heat stability (Jiang et al., 2012). In order to produce high performance and affordable polymeric materials, thermal, mechanical properties and functions of PVOH can be improved by incorporating biopolymer with other fillers (Muhammad and Zulfiqar Ali, 2018).

Recently, the composites are developed by dispersing foreign particles into a polymer matrix. Natural fillers have been introduced to biopolymer to minimize the production cost. Natural fillers can be found from industrial waste or agricultural waste such as cuttlebone, shellfish shell and eggshell. Natural fillers are selected due to their low density, high availability, renewability and low energy consumption compared to synthetic fillers. They also enhance

biodegradability but reduces overall mechanical properties. Hence, the polymer matrix is then hybridized with reinforcing filler to balance the mechanical properties of composites. Montmorillonite and calcium carbonate are the common reinforcing fillers (Nur Fazreen, Hanafi and Mohamad Kahar, 2017).

In this research, montmorillonite (MMT) and cuttlebone are used as potential reinforcing materials for PVOH polymer. MMT is the purest form of crystalline nanoclay structure available on earth. Owing to its high aspect ratio and large volume fraction of clay, only small amounts of MMT can improve mechanical and tensile strength of nanocomposites over traditional composites. MMT has the characteristics of thermal stability and big surface area for interaction with surrounding matrix (Mojtaba et al., 2015). Besides, due to the polymer intercalation, Young Modulus and percentage of elongation of nanocomposite are higher than pure PVOH polymer (Mohamed et al., 2013). MMT has hydrophilic characteristic in presence of sodium cation between interlayer. It is miscible with a water-soluble hydrophilic polymer such as PVOH. Thus, a homogeneous dispersion in a polymer matrix can be formed in this polymer-clay nanocomposites (Zanela et al., 2018). Furthermore, there is a huge amount of cuttlebone waste produced daily causing environmental problem. Cuttlebone is low cost and non-toxic. Hence, it is easily available to use as a filler, showing reinforcing effect such as good crystalline structure in bio composite material. Cuttlebone possesses good biocompatibility, good permeability, porosity and compressive strength (Yasmin and Kalyani, 2015).

In summary, there is no much attempt on the study of PVOH-cuttlebone-MMT composites. The purpose of this study is to determine the characteristics of PVOH-cuttlebone-MMT nanocomposites with different loading of the cuttlebone and MMT. Further investigation will be conducted in this research.

1.2 Problem Statements

Recently, there are trends in blending materials that are renewable and biodegradable with polymers. The nanocomposite was reinforced PVOH-MMT by improving the physical, mechanical and thermal properties. Cuttlebone was

then used as a reinforcing material to reduce the cost. The research study was conducted to examine the characterisation of polyvinyl alcohol with cuttlebone and MMT composite material. In this study, different amounts of calcined cuttlebone had been added into PVOH-MMT composite to monitor the changes of properties. The following problem statements of this study were identified:

1. What are the effects of calcined cuttlebone and MMT in PVOH-cuttlebone-MMT nanocomposites in terms of mechanical strength and morphologies of composites?
2. What are the extent of crystallinity, chemical interaction and thermal properties of PVOH-cuttlebone-MMT composites?

1.3 Objectives

This study was to determine the characterisation of polyvinyl alcohol added with calcined cuttlebone and MMT composites material. PVOH polymer was blended with different loading of MMT and cuttlebone. Hence, this study was to examine the optimal combination of MMT and cuttlebone added to PVOH polymer. The objectives of the study were identified as follow:

1. To evaluate the effect of calcined cuttlebone and MMT in PVOH-cuttlebone-MMT in terms of mechanical strength and morphologies of composites.
2. To investigate the crystallinity, bonding interaction and thermal properties of each blended composite.

1.4 Scope of Study

This study was divided into two main categories, which were the preparation of PVOH-cuttlebone-MMT composites and characterisation of PVOH-cuttlebone-MMT composites. PVOH polymer was blended with different loading of MMT and cuttlebone using the casting method. Several tests were carried out to characterise the composites as follow:

1. Tensile Test

The mechanical properties such as Young Modulus, tensile strength and elongation of PVOH-cuttlebone-MMT composites were measured. These tests were carried out in accordance with ASTM D882 standard.

2. X-ray Diffraction (XRD) Test

XRD was carried out to investigate the crystalline structures and the dispersion of cuttlebone and MMT in PVOH matrix.

3. Scanning Electron Microscopy (SEM) Observation

The morphologies of PVOH-cuttlebone-MMT composites were observed.

4. Fourier Transform Infrared Spectrometry (FTIR) Test

Bonding interaction in the polymer matrix of the composite materials was analysed.

5. Differential Scanning Calorimetry (DSC) Test

The thermal properties of PVOH-cuttlebone-MMT composite were evaluated.

CHAPTER 2

LITERATURE REVIEW

2.1 Polyvinyl Alcohol (PVOH)

Polyvinyl alcohol is a semi crystalline or linear synthetic polymer. Polyvinyl alcohol is known as PVOH, PVA or PVAL. It can be in granular or powdered form with a creamy or whitish appearance. It is also tasteless, odourless and benign to the human body. PVOH possesses characteristics of ductile, strong, hard, thermoplastic, viscous and flexible. Main chains of PVOH are joined by C-C bonds (Gaaz et al., 2015). Descriptions of natural properties of PVOH are presented in Table 2.1 below.

Table 2.1: Summary of PVOH (Muhammad and Zulfiqar Ali, 2018).

Nature Properties	Description
Melting point	180 °C to 190 °C (for partially hydrolysed PVOH) 230 °C (for fully hydrolysed PVOH)
Boiling point	228 °C
Glass transition temperature	75 °C to 85 °C
Bulk density	641 kg.s/m ³
Density	1.19 g/cm ³ to 1.31 g/cm ³
Thermal stability	Decomposition rate at 200 °C
Stability to sunlight	Excellent
Flammability	Burn like paper

2.1.1 Chemical structure of PVOH

PVOH consists of repeating macromolecules, which are produced from polyvinyl acetate through hydrolysis or saponification. Vinyl acetate is used as raw material during the polymerisation process where the hydroxyl group in aqueous sodium hydroxide environment partially takes over the ester group of vinyl acetate. PVOH is then precipitated after adding saponification agent gradually. The structural monomer, vinyl alcohol is replaced by vinyl acetate due to its unstable nature. The length of the period of saponification process

determines the extent of hydrolysis of PVOH with different attributes of polyvinyl acetate (Gaaz et al., 2015).

PVOH has an empirical formula of $(C_2H_4O)_n(C_4H_6O_2)_m$ with molecular weight of 20 000 g/mol to 400 000 g/mol. PVOH can be categorized into two groups, which are partially hydrolysed and fully hydrolysed (Lim, 2018). It also has structural formula of $(-CH_2CHOH)_n(-CH_2CHOCOCH_3-)_m$ for partially hydrolysed PVOH and $(-CH_2CHOH)_n$ for fully hydrolysed PVOH. Abundant hydroxyl groups modify the properties of PVOH. The partially hydrolysed PVOH has different properties than the fully hydrolysed PVOH. The fully hydrolysed PVOH is greatly preferable to partially hydrolysed PVOH. This is because fully hydrolysed PVOH has higher crystalline materials that lead to stronger mechanical properties. Hydrogen bonds inhibit the motion of PVOH matrix. Hence, fully hydrolysed PVOH has higher rigidity and higher strength (Gaaz et al., 2015).

2.1.2 Properties of PVOH

The number of hydroxyl groups present in the PVOH polymer determines the degree of hydrolysis of PVOH. PVOH contains polar alcohol groups that will form hydrogen bonds with water. Hence, PVOH is soluble in water but insoluble in ketones, aliphatic and aromatic hydrocarbons, esters and oils. Owing to its hydrophilic properties, degradation of PVOH can be aided through hydrolysis. It shows that PVOH has good biodegradability because there are hydroxyl groups on carbon atoms (Gaaz et al., 2015).

PVOH has characteristics of good chemicals and heat resistance. However, it has disadvantages of low decomposition temperature, high glass transition temperature and low elongation at break. Besides, it also possesses good conductivity with high dielectric strength. Furthermore, it has properties of thermal stability used in optoelectronic and other applications. PVOH possesses oxygen or aroma barrier properties by eliminating the moisture inside to combat disruption in gas permeability. It is also effective in film forming and emulsifying. Therefore, PVOH can be used as crosslinking by blending with nanofiller and other polymers (Soundararajah, Karunaratne and Rajapakse, 2010).

If there is an increasing molecular mass of PVOH, the tensile strength, crystallinity and adhesion will increase, flexibility will decrease. The crystal structure of PVOH is varied with hydrogen bonding patterns.

2.1.3 Application of PVOH

Various grades of PVOH are available on the market depending on the molecular mass, viscosity and level of hydrolysis percentage. It has film-forming, emulsification and adhesion barrier properties to be applied in fibres, films and adhesive agents widely. Examples are the synthesis of polyvinyl butyral (PVB) and vinylon fibres. PVB is the adhesive agents applied in shape memory devices and safety glass laminating vehicles whereas vinylon is the synthetic fibre applied in textiles, quilts wadding, ropes and shoes. PVOH can be widely used in diverse application such as paper making, 3D printing, water filtration, freshwater sports fishing, toxic metals absorption and batteries/ fuel cells membranes. In the food packaging industry, it can also be applied in coating for food supplements which is non-toxic. Besides, it has semi-crystalline nature with hydrogen bonding between PVOH chains. PVOH exists in different morphologies to be applied in pharmaceutical, biomedical such as scaffolds. PVOH also have good optical quality to make optical sensors and optoelectronic devices (Muhammad and Zulfiqar Ali, 2018).

2.1.4 Morphologies of PVOH

Since the PVOH matrix is explored, there are various morphologies studied such as bulk PVOH, PVOH hydrogels, PVOH beads, PVOH fibres, PVOH films, PVOH membranes and PVOH scaffolds (Muhammad and Zulfiqar Ali, 2018).

2.1.5 PVOH in Polymer Nanocomposite

There are poor resistance and insufficient mechanical properties in solvent for pure PVOH. PVOH also has insufficient strength, low heat stability and anti-ageing behaviour. PVOH-based nanocomposites are then developed to improve the mechanical, thermal and permeability properties. PVOH is an expensive material. In order to reduce the cost of material, PVOH is doped with low-cost nanofiller such as montmorillonite. Natural filler like cuttlebone as

reinforcement agent can be incorporated in polymer composite to enhance the mechanical properties of the film (Muhammad and Zulfiqar Ali, 2018).

2.2 Montmorillonite (MMT)

Nano-clays are nanoparticle of layered mineral silicates. The sheet-structured hydrous silicates are known as phyllosilicates. Nano-clays can be organized into several types such as smectite group, kaolinite group, illite group and chlorite group. Montmorillonite (MMT) is a type of smectite group where two silicate layers are sandwiched with one aluminium hydroxide layer in same stacking arrangement. Table 2.2 below shows the natural properties of MMT (Gutierrez, 2018). There are various colours for MMT due to the substitution of cations in the interlayer within the lattice structure.

Table 2.2: Summary Descriptions of MMT (Gutierrez, 2018).

Properties	Description
Density	2 to 3 g/ cm ³
Crystal system	Monoclinic
Hardness	1 to 2 Mohs scale, soft, possess fine-grained occurrence
Fracture	Irregular, uneven
Cleavage	Perfect
Lustre	Earthy, dull

2.2.1 Chemical Structure of MMT

MMT consists of 1nm thick phyllosilicate with 10 μ m sized multi stacks. Based on Figure 2.1 below, MMT has crystalline lattice with constitutions of octahedral and tetrahedral sheets. The tetrahedral sheets consist of silicon-oxygen tetrahedra linked to neighbouring tetrahedra by sharing three corners to form a hexagonal structure, interconnected by hydroxyl group to adjacent octahedral sheet of alumina or magnesia. These two sheets form a layer together has chemical formula of (Si₂O₅)⁻² with ratio of 2:1 (Tetrahedric: Octahedric: Tetrahedric). Moreover, the water molecules and cations (Na⁺ and Ca⁺) fill the gallery or interlayer, which is the space between two stacks. The basal space is the addition of length of a layer and length of a gallery.

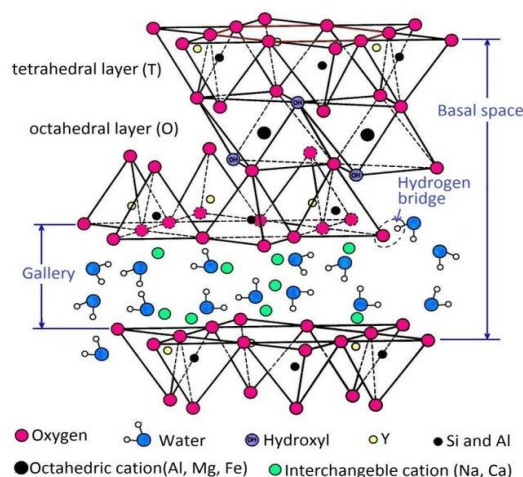


Figure 2.1: The Crystalline Structure of MMT (Gutierrez, 2018).

There are various types of bonding in the MMT crystalline structure. One of them is Van der Waals force that keeps the stacks together. The other types of bonding are the electrostatic force and hydrogen bonding. The electrostatic force is the weak force between the sheets. Phyllosilicates separate or exfoliate their sheets in a parallel way because Van der Waals forces are much weaker than forces generated by ions located in the interlayer (Gutierrez, 2018).

Furthermore, cation exchange occurs when the positively charged ions possessed by the negatively charge of MMT clay materials. The quantity is measured in unit of meq/g. Isomorphous substitution affects the layered structure because it replaces a component with another component in mineral crystal and not modifies chemical structure. Fe^{3+} and Al^{3+} are tiny enough to substitute Si^{4+} in tetrahedral coordination with oxygen whereas Mg^{2+} , Fe^{2+} and Fe^{3+} substitute Al^{3+} in octahedral coordination. The produced imbalance negative charges are then compensated by the large size cations such as K^+ , Na^+ and Cs^+ at interlayer. Electric charge equilibrium is achieved by interacting metallic oxides with cations (Thakur, Singh and Singh, 2016).

The chemical composition of MMT varies due to the imbalance charge by cation substitution. But the structure in any form composes of water molecules. Besides, the elementary molecular structure depends on unit comprising silica tetrahedron and aluminium octahedral. The cation Si^{4+} is fourfold and holds tetrahedral coordination with oxygen whereas the cation Al^{3+} happens in sixfold or octahedral coordination (Andreas, Fotios and Nick, 2011).

2.2.2 Properties of MMT

MMT is the most common natural silicate used in diverse application. It is cost-effective and available porous material. MMT has characteristics depends on chemical composition, ionic substitution, layered structure and particle size of natural clay minerals (Andreas, Fotios and Nick, 2011).

MMT is a fine-grained small particle of clays with less than 2 mm size. It has high aspect ratio (10 to 1000) when the diameter of particle is lesser than the length, contributing to higher specific surface area of MMT (between 60 and 300 m²/ g).

MMT has the characteristics of high cationic interchange capacity (60 and 200 meq/ 100g, the highest value in clays). This is because when the surface area per unit mass increases, more cations can be absorbed to impart the electrical conductivity in clay. It also has environment compatibility and capability to improve mechanical strength, decrease the water vapour permeability and progress the polymer film efficiency as dressings. Besides, MMT functions as a flame retardant and heat resistant.

MMT possesses various water sorption based on the humidity content in the ambient environment. High surface area per unit mass of MMT is exposed when the water fills the space between the silicate layers. There is an interaction between water particles absorbed and montmorillonite nanoclay. Swelling behaviour also happens in montmorillonite, forming hydrated states and hysteresis. Meanwhile, dehydration occurs when there is a loss of water and phase changes to stronger nonexpendable clay.

MMT also has high thermal stability, resulting in low thermal expansion. The aspect ratio should also be increased greater than 100. Thermal expansion has a decreasing order from polymer, metal and ceramic.

2.2.3 Application of MMT

MMT is auspicious in diverse application. It can enhance the performance of materials and products in catalysis, food additive and polymer manufacturing.

It has an antibacterial function which is resistant to tooth decay, nausea and diarrhoea. There are some aspects of drug carrier system includes analysis for a sustained drug release, drug loading and entrapment, targeted drug release

and molecular-level interactions. Besides, MMT can be applied in the absorption of dyestuff and toxic heavy metals.

2.2.4 Comparison between MMT with Other Silicates

Layered silicates in pure state are hydrophilic and nanolayers are difficult to disperse in most polymers, leading to formation of agglomerates. The intrinsic incompatibility of hydrophilic layered silicates and hydrophobic engineering plastics hinder the dispersion of the inorganic platelets into discrete monolayers. Layered silicates are rendered to be miscible with hydrophobic polymer matrices by converting the hydrophilic layered silicate to organophilic, so that there is more effective in intercalation of polymer chains into inorganic galleries.

By comparison, MMT is a miscible inorganic material which contains hydrated Na^+ or K^+ ions. MMT is able to form stable suspensions in water and promote dispersion of inorganic crystalline layers in water-soluble polymers such as PVOH, polyethylene oxide due to its hydrophilic character.

2.2.5 MMT in Polymer nanocomposite

MMT is the raw material used to produce nanoclays. It is hydrated sodium calcium aluminium magnesium silicate hydroxide with chemical formula of $(\text{Na Ca})_{0.33} (\text{Al Mg})_2 (\text{Si}_4\text{O}_{10}) (\text{OH})_2 \text{nH}_2\text{O}$ (Elbadawy et al, 2015). The hydroxyl groups and charges exist in MMT determine the interaction between nanoclay particles and polymer matrix. Although MMT nanoclay has ultrafine size range with toxic properties, particles embedded in the polymer will not exhibit this poor effects to health. Polymer Layered Silicates nanocomposite (PLS) has the enhanced mechanical and barrier properties to improve its performances due to its potentially high aspect ratio and surface area. Nano-size MMT is very effective even it is only applied in small amounts (Gaidukov, Danilenko and Gaidukova, 2015).

The degree of dispersion of clay in polymer matrix detects the structure and the final properties of the composites. There are three types of clay-polymer nanocomposites, which are non-mixing conventional composites, intercalated structure and exfoliated structure. As shown in Figure 2.2 below, intercalation occurs when polymer chains are embedded between the clay platelets as nanoparticle in well-order multilayer whereas exfoliation occurs when silicate

layers are well-dispersed in organic polymer. The silicate of exfoliated structure is not in order as in intercalated structure. Meanwhile, phase-separated microcomposite has weak interactions between clay particles and polymers. The polymers cannot get in clay galleries and poor mechanical properties are possessed.

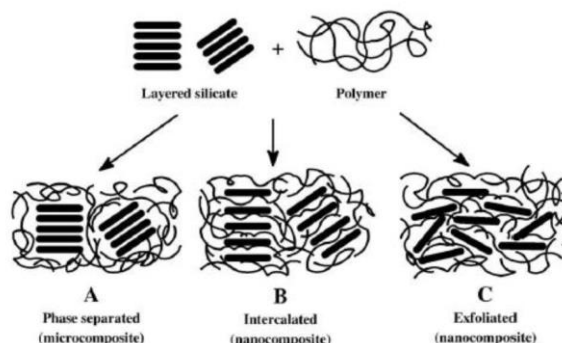


Figure 2.2: Types of composite structures (Ling, 2015).

2.3 Cuttlebone

Cuttlebone has the name of *Sepia Officinalis*. It is also known as cuttlefish bone. It contains the compositions of inorganic coralline CaCO_3 (around 93 %) and organic components such as protein and chitin (around 6 %) (Poompradub et al., 2008). The organic layer coats the inorganic ceramic. The mineralisation of inorganic material will be initiated and inhibited. It has a similar concept with buoyancy tank to aid cuttlefish to float in seawater (Birchall and Thomas, 1983). As shown in Figure 2.3, there are two major parts of cuttlebone, which are a dorsal shield that represent a cover for lamellar matrix and internal lamellar matrix which consists of chamber-shaped porous structure (Cadman et al., 2012).

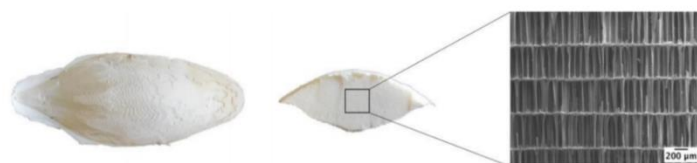


Figure 2.3: Cuttlebone's Section and the Scanning Electron Microscopy of Dorsal Field and Lamellar Matrix (Birchall and Thomas, 1983).

There are large amounts of cuttlebone wastes are generated in massive quantities in food industries daily, which create many environmental problems

such as odour produced (Ferro and Guedes, 2019). The skeleton of cuttlefish is discarded after use. Cuttlefish bone is chosen as calcium sources for more than 90 % to promote recycle of materials (Ferro and Guedes, 2019). Hence, cuttlebone waste can be used as a reinforcement agent to eliminate these biomass waste and other disposed-related issues (Mostoufi, 2016). Cuttlebone is easily available and abundant in nature (Faksawat et al., 2015). It is lightweight and low-cost material with unique porous microstructure (Florek et al., 2009). It possesses combination mechanical properties of high stiffness, high porosity, high biocompatibility and high permeability. In term of mechanical and chemical properties, it has toughening effect of organic material (Rocha et al., 2005).

In present work, there are few attempts that the polymer is reinforced by cuttlebone bio-filler to develop polymer composites (Shang et al., 2014). Interaction between filler and matrix and mechanical properties in polymer composites were expected to be improved. Cuttlebone has an exceptional framework and high strength to weight ratio. The efficiency of reinforcing filler based on aspects such as particle size, surface area and shape of filler. The density of cuttlebone is 2.70 g/cm^3 with an aragonite form of CaCO_3 crystal structure (Cadman et al., 2012).

2.3.1 Chitosan

The cuttlebone acts as reinforcing filler because of the presence of B-chitin, which is composed of N-acetyl-D-glucosamine units (Wang et al., 2005). Chitosan is a biopolymer obtained by deacetylation of chitin from crustacean's species. It is a film-forming material which involves reactivity among the hydroxyls and the amino groups. Small amounts of clay minerals such as montmorillonite are mixed with chitosan as composite to enhance the mechanical properties and improve the thermal behaviour of chitosan film (Mourak, Hajjaji and Alagui, 2019).

2.3.2 Hydroxyapatite (HAP)

$\text{Ca}_{10}(\text{PO}_4)_6(\text{OH})_2$ is the chemical formula of hydroxyapatite (HAP) (Thakur, Singh and Singh, 2016). Cuttlebone which contains calcium carbonate can be utilised as a source of calcium oxide to synthesize value-added HAP. HAP can

be produced by adding phosphoric acid or ammonium hydrogen phosphate (Sarin et al., 2011). It is calcium phosphate ceramic that has similar compositions and structure as bones and teeth. HAP can be produced as bone scaffold material when undergoing calcination treatment at 1000 °C for 1 hour (Ashwin, Karthick and Arumugam, 2011).

Because of its versatility, it is used in various fields like wastewater treatment, bone tissue engineering and biomedical application. HAP is also a good absorbent. It is highly stable under reducing and oxidising conditions. Besides, it has appropriate characteristics like surface charge, hydrophilicity, porosity, surface functional groups, acidity and basicity. It has excellent properties such as biocompatibility, exceptional mechanical strength and osteoconductivity (Sinha et al., 2007). It is bioactive and non-immunogenic and does not exhibit any cytotoxic effects (Kar, Kaur and Thirugnanam, 2016).

Figure 2.4 shows the treatment of calcination temperature affects the exchange of cation and anion during the calcination process. This is because the ions have valence electron tend to achieve equilibrium. Calcination time also affects the crystallinity and amorphous membranes. The percentage of calcination temperature increases, the crystallinity phase tends to increase, the amorphous phase tends to decrease. The formation of amorphous phases is caused by the presence of impurity elements which can alter the chemical structure of compounds. These compounds will be evaporated when calcination temperature increases. Besides, the higher the crystallinity, the higher the mechanical strength of bone scaffold materials (Henggu, Ibrahim and Suptijah, 2019).

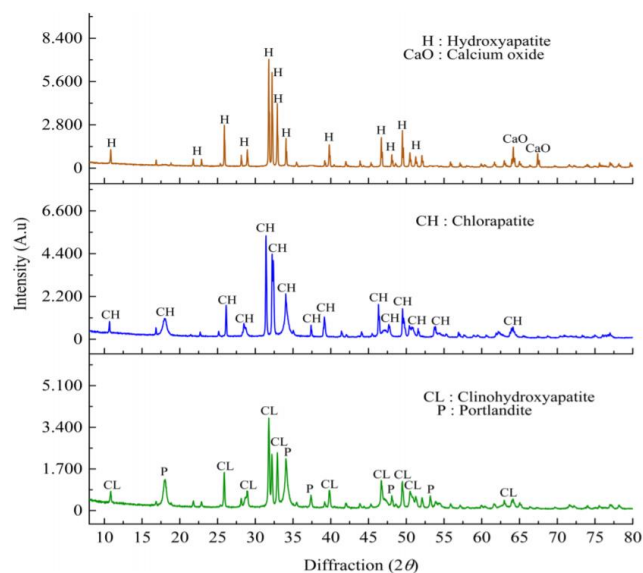


Figure 2.4: Diffractogram of apatite structure with different calcination temperature treatments (green (800 °C), blue (900 °C), red (1000 °C)) (Henggu, Ibrahim and Suptijah, 2019).

2.4 PVOH-MMT nanocomposites

According to Gaidukov, Danilenko and Gaidukova (2015), for PVOH-MMT blends, MMT nanoclays were added into the PVOH matrix. MMT filler was explored significantly because it could form exfoliated or intercalated composites when added to PVOH. MMT was required in small quantity only to achieve certain extent of stiffness and strength. Besides, PVOH-MMT blends had lamina structure. The hydrogen bonding interaction between PVOH and MMT layers were strong. Macromolecule-nanoparticle interactions helped to modify the crystalline structure of PVOH. Mechanical properties of PVOH-MMT nanocomposites would be enhanced.

Furthermore, PVOH-MMT had intercalation and exfoliation due to the type of polymer and hydrophilicity and surface energy MMT as shown in Figure 2.5. Na⁺ MMT had better mechanical and thermal properties of neat PVOH before degradation and agglomeration occurred. When there was a small particle distance of MMT, barrier performance was improved (Bee et al., 2014).

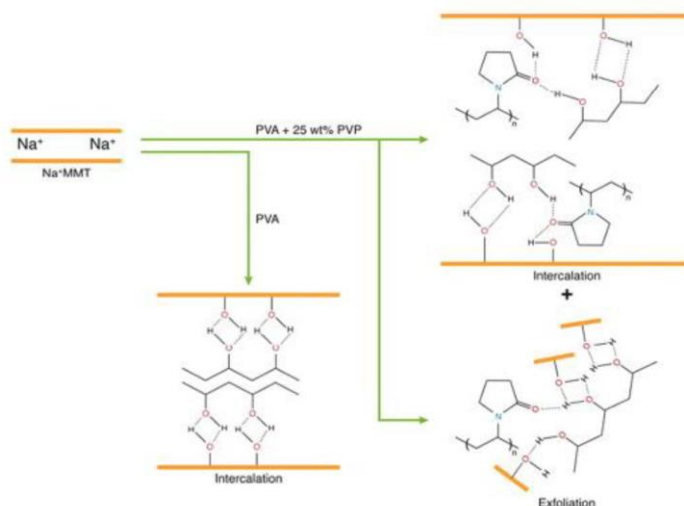


Figure 2.5: Intercalation and Exfoliation of Na^+ MMT on PVOH (Ooi, 2017).

2.4.1 Tensile Test

Based on Allison et al. (2015), mechanical properties such as Young Modulus and elongation values were tested during the tensile test. Intercalation of MMT could be observed. The loading of MMT was transferred to the silicates. The hydrogen bonding was then formed on the hydrophilic surface of MMT to bind strongly with polymer matrix. Besides, Young Modulus was directly proportional to the various amount of MMT can be shown in Figure 2.6.

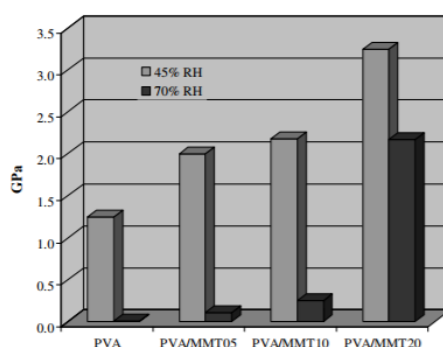


Figure 2.6: Mechanical Properties of Developed Nanocomposites with Various Amount of MMT in term of Young Modulus (Allison et al., 2015).

However, when a higher amount (≥ 2.5 phr) of MMT was added to PVOH, the poor dispersion of MMT occurred in polymer matrix. There was inverse relationship in Young Modulus where MMT was not distributed homogeneously. Agglomeration of MMT happened causing stress

concentration in polymer matrix during extension process. PVOH matrix was less intercalated into MMT galleries due to the damage of continuity of PVOH matrix by phase separation. Mechanical performance of composite was weakened (Allison et al., 2015).

Furthermore, pristine PVOH had the highest value of elongation compared to other PVOH-MMT composites based on Figure 2.7 (Gaidukov, Danilenko and Gaidukova, 2015). This was due to the neat PVOH could slide freely during extension process. Elongation was decreased when loading level of MMT increased. Agglomeration happened when MMT was clustered and distributed unevenly. This caused the blockage of the smooth of PVOH. The reinforcing effect of MMT was then reduced (Bee et al., 2014).

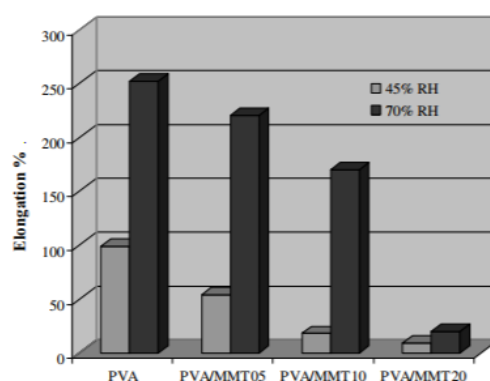


Figure 2.7: Mechanical Properties of Developed Nanocomposites with Various amount of MMT in term of Elongation Value (Allison et al., 2015).

However, when a higher amount (≥ 3.5 phr) of MMT was added to PVOH, the elongation of PVOH-MMT increased. MMT helped to lubricate PVOH matrix. MMT and PVOH matrix could slide with each other. Owing to the hydrophilic characteristic of MMT, the elongation at break was further enhanced by lubricating the inter-chain PVOH-MMT composites (Bee et al., 2014).

2.4.2 SEM

Based on Bee et al. (2014), the surface morphologies of neat PVOH and PVOH-MMT blends were analysed. In Figure 2.8 (b), it could be shown that globules were formed because the chains realigned themselves after elongation due to the

elasticity effect of PVOH. Fibrils were also observed because PVOH matrix had resistance to elongation due to the straining effect of PVOH. A similar appearance was also seen in PVOH-MMT nanocomposites. The flakes presented in the matrix because MMT particles were not distributed homogeneously in PVOH resins. Agglomeration of MMT particles restricted motion of PVOH chains during recrystallization. As a result, flakes (agglomerated particles) were observed the most in the highest loading level of MMT. The agglomeration effect of MMT particles increased with the increasing loading level of MMT in PVOH matrix. The lower amount of MMT was distributed homogeneously than the higher amount of MMT in composite.

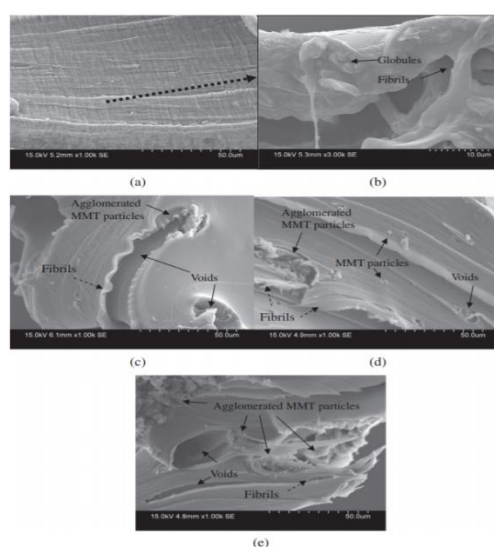


Figure 2.8: Surface morphologies of fractured surface for (a) Neat PVOH ($\times 10\ 000$), (b) Neat PVOH ($\times 30\ 000$), (c) PVOH composites with added 0.5 phr MMT ($\times 10\ 000$), (d) PVOH composites with added 1.5 phr MMT ($\times 10\ 000$), (e) PVOH composites with added 4.5 phr MMT ($\times 10\ 000$) (Bee et al., 2014).

2.4.3 XRD

According to Bee et al. (2014), MMT had characteristic diffraction peak of 5° . After adding MMT into the PVOH matrix, MMT had the clear diffraction peaks at 7° whereas PVOH had a crystalline structure with diffraction pattern from 15° to 25° . PVOH-MMT composites had smaller diffraction angles of 2θ and higher interlayer distance. Modification of polymer crystal structure caused the change

of shape of peak. The macromolecular chain mobility was restricted due to the absorption of MMT layers and development of strong bond interaction. More crystallinity phases occurred in PVOH-MMT composites due to nucleating effect of MMT particles to change the overall polymer crystalline structure. PVOH-MMT had increased intensity compared to pristine PVOH.

The nanostructure of MMT particles could be measured and observed using XRD. Based on Figure 2.9, there were two observed peaks, which were peak A and peak B. Both peaks for PVOH-MMT composites were shifted to lower 2θ . The peaks could be observed on XRD curves compared to peaks of pristine MMT. This showed that PVOH is intercalated excellently into MMT fillers (Bee et al., 2014).

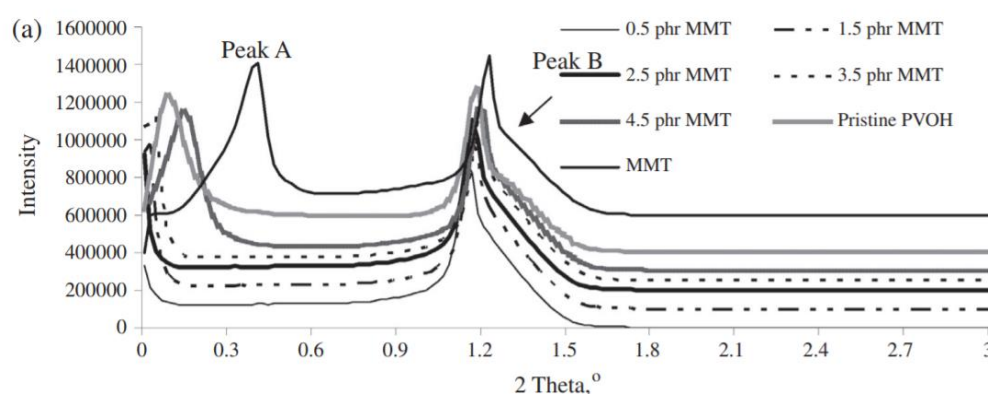


Figure 2.9: XRD Curves ($0^\circ \leq 2\theta \leq 3^\circ$) for PVOH with Different Loading Level of MMT (Bee et al., 2014).

Specimens were oriented on the substrate to delineate the basal spacing of clay in composites. Based on Table 2.3 at Peak B, d-spacing values of all PVOH-MMT blends were slightly higher compared to neat MMT. PVOH-MMT composites were arranged by shifting peak B causing increased d-spacing. The intensity increased because of the large amount of clay in composite. The distance between interlayers of MMT fillers increased because PVOH matrix was intercalated into interlayer galleries (Bee et al., 2014).

Table 2.3: Inter-chain Separation and d-spacing of Neat PVOH and PVOH-MMT blends on Peak B (Bee et al., 2014).

Loading level of MMT, phr	2θ, °	d-spacing, Å	Δd, Å	Inter-chain separation, Å
0.0	1.2458	70.9	-	88.6
0.5	1.1938	74.0	3.1	92.5
1.5	1.1965	73.8	2.9	92.3
2.5	1.2131	72.8	1.9	91.0
3.5	1.2166	72.6	1.7	90.8
4.5	1.2216	72.3	1.4	90.4

Furthermore, with increased amounts of MMT, inter-chain separation of PVOH-MMT composites decreased and separation distance between MMT in PVOH matrix increased. This is because MMT was well-distributed in the PVOH matrix (Bee et al., 2014).

However, when MMT loading level in the PVOH matrix increased from 0.5 phr to 4.5 phr, d-spacing decreased. MMT particles at higher loading level tended to agglomerate together. MMT particles were not easily intercalated in PVOH matrix. Besides, a well-ordered composite was produced when there was lower amount (≤ 0.5 phr) of MMT. Therefore, with higher amount of loading level of MMT, a saturation state was reached. It could not achieve full intercalation of MMT with PVOH matrix (Bee et al., 2014).

2.4.4 FTIR

Interaction between the components was characterised. Figure 2.10 shows FTIR spectra measured in the range of 500-4000 cm^{-1} for PVOH, MMT and PVOH-MMT samples. There were characterisation absorption peaks of PVOH at 850 cm^{-1} (C-C stretching vibration), 916 cm^{-1} (CH_2 rocking vibration), 1096 cm^{-1} (C-O stretching vibration), 1141 cm^{-1} (C-C and C-O-C stretching vibration), 1430 cm^{-1} (CH_2 bonding vibration), 2942 cm^{-1} (C-H stretching vibration) and 3330-3340 cm^{-1} (O-H stretching vibration). For MMT, it had characteristic bands at 525 cm^{-1} and 470 cm^{-1} (Al (Mg)-O-Si), 796 cm^{-1} (Al (Mg)-O-H), 920

cm^{-1} (Al-O-H) and $1040\text{-}1120\text{ cm}^{-1}$ (Si-O). Combined peaks had been shown in the spectrum of PVOH/ MMT blends. A broad band, O-H vibration at $3300\text{-}3700\text{ cm}^{-1}$ showed that there was a presence of O-H groups to form hydrogen bonding between the components. Besides, ratio of intensities of absorption bands was used to calculate the crystallinity degree of PVOH and PVOH-MMT composites. The crystallinity degree was increased when MMT was added to the PVOH matrix compared to pure PVOH as shown in Table 2.4. The strong interaction between PVOH and MMT was formed (Gaidukov, Danilenko and Gaidukova, 2015).

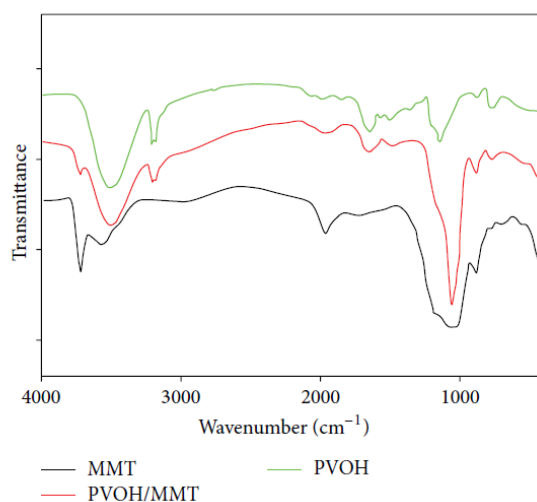


Figure 2.10: FTIR Spectrums of PVOH, MMT and PVOH-MMT Blends (Gaidukov, Danilenko and Gaidukova, 2015).

Table 2.4: Crystallinity Degree and Melting Temperature of PVOH and PVOH-MMT Composite (Allison et al., 2015).

	X^{FTIR} , %	Melting Temperature, °C
PVOH	48.7	226.5
PVOH-MMT	69.1	273.1

2.4.5 TGA

The decomposition rate of composites was identified using TGA. Figure 2.11 shows a reduction of weight loss for nanocomposites and pristine PVOH at different volume fraction. There were three distinct peaks in TGA curve. The first peak referred to water evaporation at ambient temperature from 183 °C to

200 °C. The second peak was the first step degradation of PVOH-MMT composite whereas the third peak was the second step decomposition at around 440 °C. It indicated that when the concentration of MMT increased in nanocomposites, decomposition rate decreased, the higher the thermal resistance of composites. This is because exfoliated and intercalated MMT was dispersed in PVOH matrix. MMT particles acted as barriers to maximize heat insulation. Exfoliated and intercalated MMT was dispersed in PVOH matrix, leading to the increased melting temperature as shown in Table 2.4. This is because MMT layers had the nucleation effect. MMT was able to change the quality and quantity in the crystalline structure (Allison et al., 2015). Besides, nanocomposites had higher melting temperature compared to pristine PVOH. The nanocomposites were reinforced by adding thermal stability of intercalated PVOH. They had resistance to degradation as well as their heat resistance. After 600 °C, flat curve was observed. Inorganic residues mainly remained in PVOH-MMT nanocomposites and pristine PVOH. The mass loss of nanocomposites was higher than pristine PVOH (Mohamed et al., 2013).

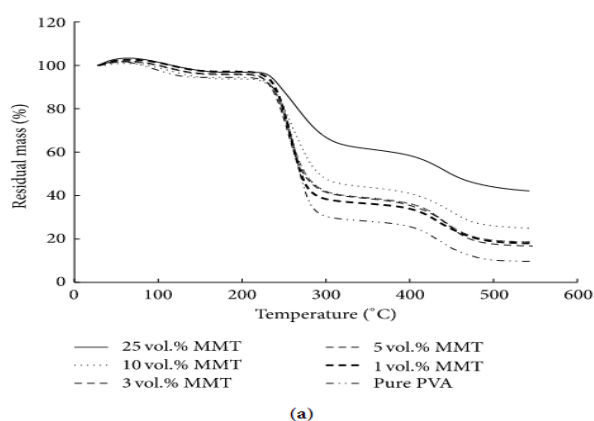


Figure 2.11: Decomposition Rate of the Material as a Function of Clay Volume Fraction (Allison et al., 2015).

2.4.6 DSC

The endotherm in DSC curve could be related to the glass transition temperature (T_g) (Mohamed et al., 2013). Ali et al. (2013) reported that PVOH-MMT nanocomposites had higher T_g compared to pristine PVOH. The PVOH chains were intercalated into the MMT layers and PVOH chains. PVOH chains were

immobile since the PVOH chains were well-dispersed within the MMT clay. Furthermore, the endotherm in DC curve could also be related to the crystalline melting point (T_m) (Mohamed et al., 2013). Based on Figure 2.12, at 210 °C, an endothermic peak could be observed due to the presence of the new crystal phase for all PVOH-MMT composites. This peak showed that the inorganic layers were well dispersed in polymer as the enthalpy of fusion of this peak was linearly with the amount of clay (Allison et al., 2015). Hence, when the MMT content increased, the crystallinity of PVOH decreased. Besides, the crystalline phase of all PVOH-MMT composites was higher than pristine PVOH. It could be concluded that PVOH-MMT was strong, highly crystalline and highly thermal stability (Allison et al., 2015).

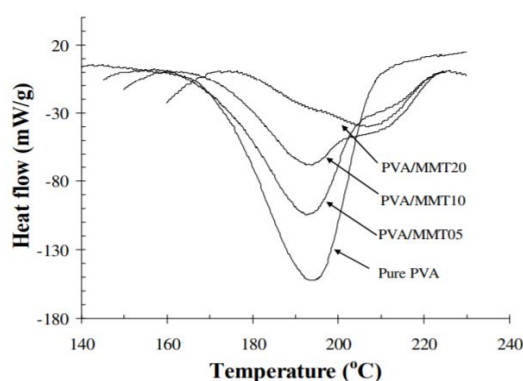


Figure 2.12: DSC curves of pure PVOH and PVOH-MMT nanocomposites (Allison et al., 2015).

2.5 Natural Rubber-Cuttlebone Composites

According to Poompradub et al. (2008), Natural rubber acted as the matrix and cuttlebone bio-filler was loaded with 5 phr to 100 phr. In the tensile test, the moduli increased with increasing loading level of filler from 20 phr to 100 phr as shown in Table 2.5. It was shown that the smaller the size of filler, the higher the reinforcement effect of cuttlebone filler. This is because the organic compounds such as chitin in cuttlebone promoted the interaction between the inorganic aragonite of cuttlebone and natural rubber. This phenomenon was also observed in SEM observation in Figure 2.13. More bright spots represented filler particles were dispersed in natural rubber matrix (black-toned colour). Besides, tensile strength at break increased with increasing filler loading up to

40 phr and then decreased up to 100 phr. It could be concluded that modulus and tensile strength at break increased, the elongation decreased in the filler-filled rubber composites.

Table 2.5: Properties of Cross-linked Natural Rubber Filled with Cuttlebone Particles (Poompradub et al., 2008).

Samples	Stress at 100% Elongation, MPa	Stress at 300% Elongation, MPa	Tensile Strength at Break, MPa
Natural Rubber	0.7	2.1	7.0
Natural Rubber added 10 phr	0.7	2.0	11.2
Natural Rubber added 20 phr	0.8	2.3	11.3
Natural Rubber added 40 phr	1.0	3.0	13.2
Natural Rubber added 80 phr	1.6	4.4	12.5
Natural Rubber added 100 phr	1.9	4.5	7.5

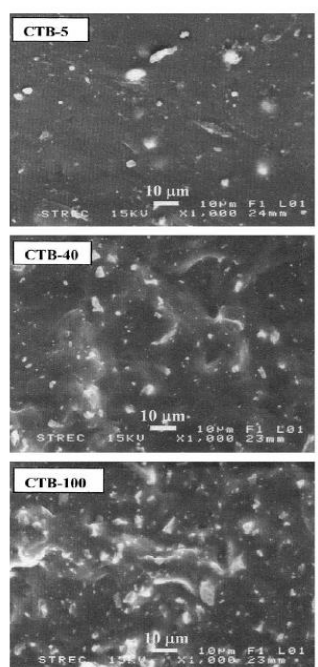


Figure 2.13: SEM Image of Cross-linked Natural Rubber Filled with 5 phr, 40 phr and 100 phr Cuttlebone Particles Filler (Darder, Colilla and Ruiz-Hitzky, 2003).

2.6 Epoxy-Cuttlebone Composites

Based on Kamalbabu and Mohan Kumar (2014), Polymer composites were prepared with epoxy as matrix and cuttlebone at different fillers contents as reinforcement.

Based on Figure 2.14 (a), the tensile strength of composite increased with increasing filler content compared to neat epoxy. This is because addition of filler would increase interface interaction between matrix and filler. Fewer voids and better stress transfer occurred in the composites. When higher loading amount of cuttlebone above critical weight fraction was added, tensile strength decreased due to the poor bonding at interface. Particles were distributed unevenly in the matrix. Based on Figure 2.14 (b), Young's Modulus of epoxy composites increased with the increasing amounts of filler. Cuttlebone had the characteristic of higher stiffness than epoxy matrix. Hence, it could be shown that the increase of filler content, the increase the Young Modulus, the increase the load carrying capacity of composites. But when it reached a certain weight ratio, modulus decreased. This is because higher particle size would cause poor adhesion between the filler and matrix. Based on Figure 2.14 (c), the increase

of filler content would increase the elongation percentage up to certain weight fraction. The elongation percentage reduced for all filler reinforced composites beyond critical weight fraction. The proper bonding was formed between filler and matrix material when the weight fraction up to 3 %. The particles were dispersed poorly in matrix. Stress concentration was created and the strain of composites was reduced. Furthermore, elongation percentage was higher in at higher filler loading. This is because high surface area and agglomeration of small particles would decrease elongation percentage (Kamalbabu and Mohan Kumar, 2014).

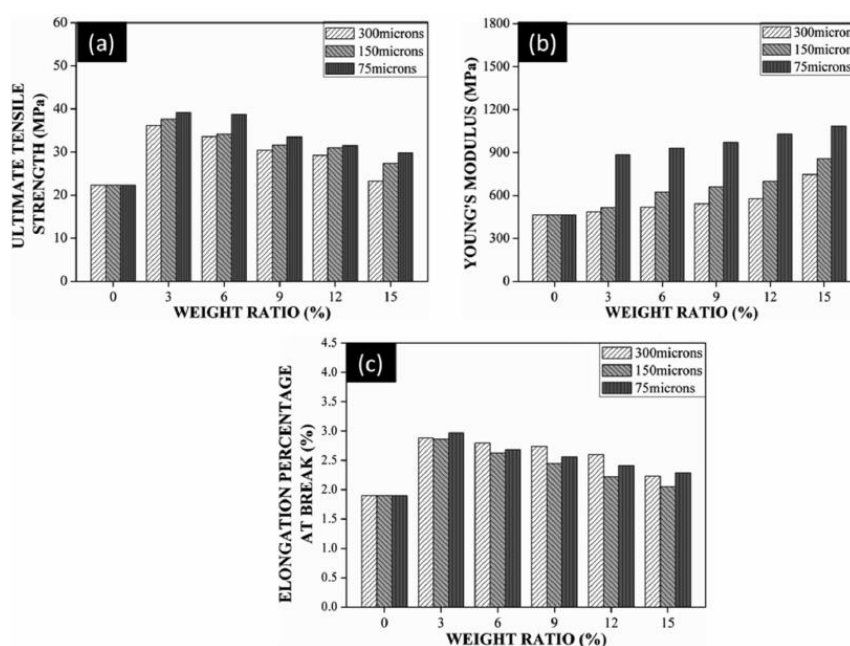


Figure 2.14: (a) Ultimate Tensile Strength, (b) Young Modulus, and (c) Elongation Percentage at Break of Cuttlebone in Different Particle Size Reinforced Epoxy Composites (Kamalbabu and Mohan Kumar, 2014).

As shown in Figure 2.15, the cuttlebone was in a flake form. In Figure 2.15 (a), neat epoxy had rough and coarse fracture surface. Once the cuttlebone was added to epoxy, the fractured surface became smooth ductile due to the uniform distribution of particles in matrix as shown in Figure 2.15 (b) (Kamalbabu and Mohan Kumar, 2014).

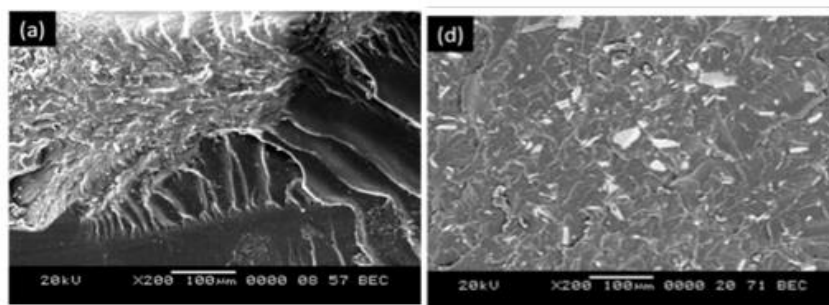


Figure 2.15: SEM micrograph of Neat Epoxy (Left) and cuttlebone in $<75 \mu\text{m}$ particle size in reinforced composites (Right) (Kamalbabu and Mohan Kumar, 2014).

As shown in Figure 2.16, there were three steps of degradation for cuttlebone. The first step of degradation happened at 25-100 °C. The moisture in cuttlebone was removed, leading weight reduction around 3 %. The next step of degradation was the decomposition of organic material at 280-320 °C with weight reduction around 8 %. At 300-350 °C, aragonite was converted to calcite polymorph form. DTA curve showed an exothermic reaction at 320 °C. The third step of degradation happened at 650-780 °C with a weight reduction of around 48 %. CaCO_3 was degraded and converted to calcium oxide (CaO) and carbon dioxide (CO_2). DTG showed the major degradation at 740 °C (Kamalbabu and Mohan Kumar, 2014).

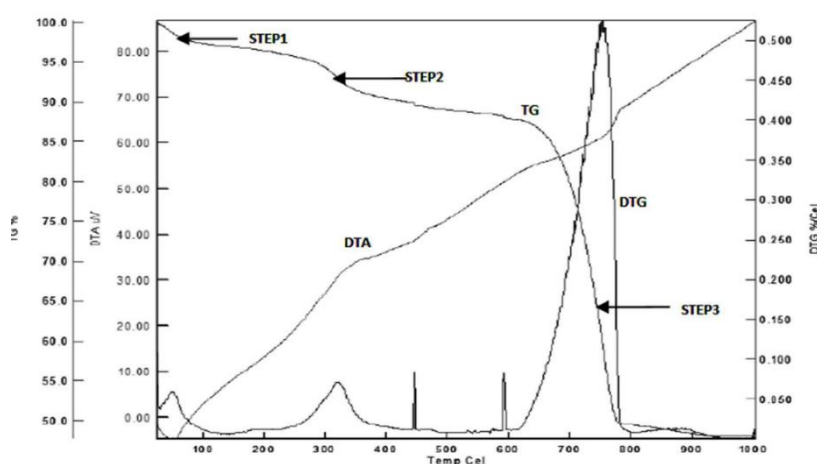


Figure 2.16: Thermal Degradation (TG), Differential Thermogravimetry (DTG) and Differential Thermal Analysis (DTA) Curves of Cuttlebone Particles (Periasamy and Kumar, 2019).

Based on Figure 2.17, epoxy-cuttlebone composites showed better thermal stability than the pure epoxy matrix. For epoxy-cuttlebone composites, thermal degradation occurred at 25-280 °C due to the presence of impurities. The uncured epoxy resin was breached. The major degradation occurred at 300-400 °C. Similarly, based on Table 2.6, T_{max} for epoxy-cuttlebone composites was higher than that neat epoxy. This indicated calcined cuttlebone filler improved the thermal stability in epoxy-cuttlebone composites due to the presence of trace amount of organic matter (Periasamy and Kumar, 2019).

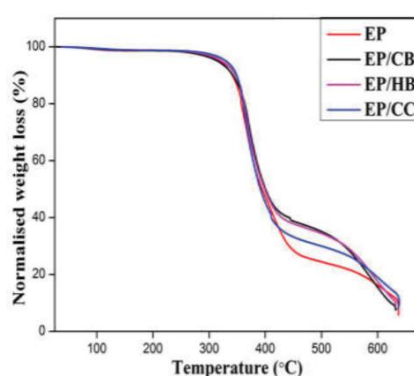


Figure 2.17: TGA Curve for Epoxy (EP), Epoxy-raw cuttlebone (EP/ CB) Composites, Epoxy-calcined cuttlebone (EP/HB) Composites, and Epoxy-commercial calcium carbonate (EP/ CC) composites (Periasamy and Kumar, 2019).

Table 2.6: Maximum Temperature (T_{max}) and Glass transition Temperature (T_g) of Neat Epoxy and Epoxy-calcined cuttlebone Composite (Periasamy and Kumar, 2019).

	Neat Epoxy	Epoxy-cuttlebone Composite
T_{max} (°C)	356.8	366.3
T_g (°C)	94.52	96.00

Glass transition temperature (T_g) and DSC curve were shown in Table 2.6 and Figure 2.18 respectively. All epoxy-cuttlebone composites had good dispersion in the matrix. The gap between the macromolecules was reduced and the epoxy had good mobility in composites. There were high cross-linking and proper adhesion between the fillers and matrix, leading to an increase of T_g

temperature. This is because there was presence of calcite polymorph structure in the reinforcement (Periasamy and Kumar, 2019).

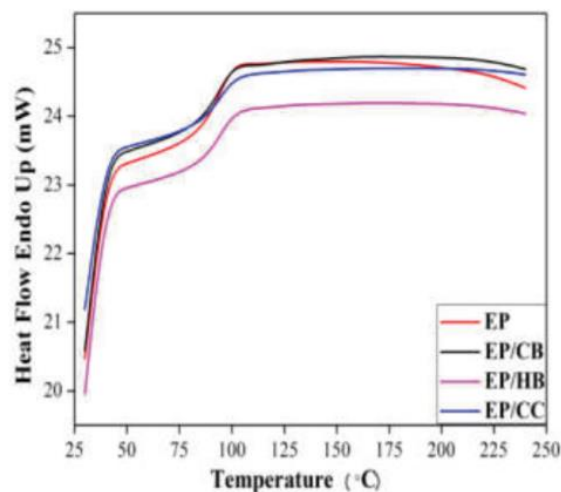


Figure 2.18: DSC Curve for Epoxy (EP), Epoxy-raw cuttlebone (EP/CB) Composites, Epoxy-calcined cuttlebone (EP/HB) Composites, and Epoxy-commercial calcium carbonate (EP/CC) composites (Periasamy and Kumar, 2019).

Based on Figure 2.19 (a) and Figure 2.19 (b), cuttlebone had CaCO_3 and chitin. It had bands of aragonite, which were ν_1 (1081.63 cm^{-1}), double ν_4 (704.63 cm^{-1} for C-O in the plane band) and ν_2 (853.34 cm^{-1}). The bands derived from internal vibrations of carbonate ions (C=O bond) were 1786 cm^{-1} and 2524.6 cm^{-1} . Chitin also observed weakly at 1030 to 1110 cm^{-1} (stretching C-O), 1652 cm^{-1} (Amide I) and 1374 cm^{-1} (Amide III). There was presence of OH and NH groups at 3200 - 3600 cm^{-1} . The peak of water molecules absented in cuttlebone spectrum (Periasamy and Mohankumar, 2016).

Based on Figure 2.19 (c), ν_1 (1081.63 cm^{-1}) and ν_2 (853.34 cm^{-1}) were disappeared. The singlet at 712 cm^{-1} was appeared instead of doublet ν_4 (704.63 cm^{-1}). When the cuttlebone was heated at $400 \text{ }^\circ\text{C}$, new peaks appeared at 712 to 875 cm^{-1} , showing that the strong aragonite structure was converted partially to calcite form. Some organic compounds did not decompose due to the strong interaction with minerals. Extensive change in grain growth required the removal of water molecules and the decomposition of organic materials.

Crystalline size of heat-treated cuttlebone was higher than raw cuttlebone. But when cuttlebone was heated above 640 °C, the volatile materials would be decomposed into CaO and CO₂. Thermal decomposition happened throughout whole cuttlebone particles. The shrinking core model was then converted to solid materials (Periasamy and Mohankumar, 2016). The organic matter band at 1652 cm⁻¹ (Amide I) was disappeared. Based on Figure 2.20, residue of calcium oxide was identified in FTIR spectra (Florek et al., 2009).

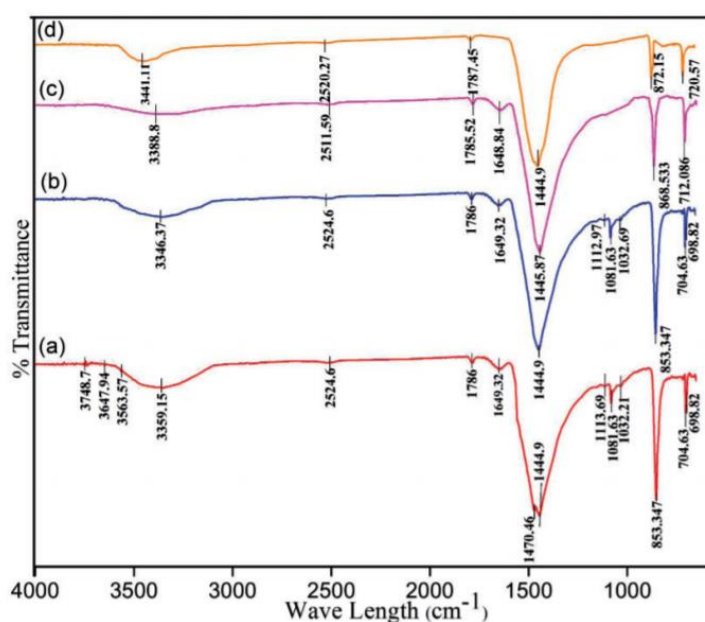


Figure 2.19: FTIR spectra of (a) Raw Cuttlebone, (b) Cuttlebone heated at 100 °C; (c) Cuttlebone Heated at 400 °C and (d) Commercial CaCO₃ (Periasamy and Mohankumar, 2016).

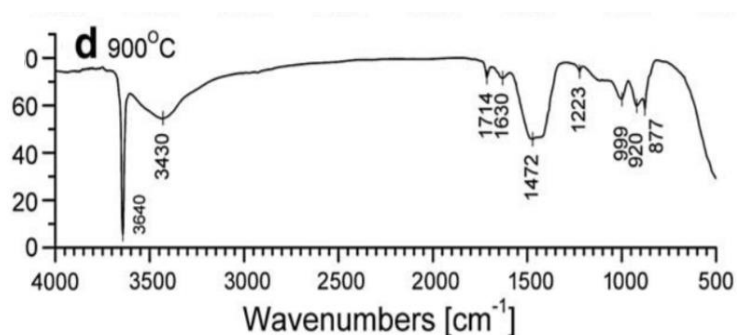


Figure 2.20: FTIR spectra of Sepia Cuttlebone at 900 °C (Florek et al., 2009).

2.7 PVOH-HAP COMPOSITES

When conducting for SEM, it could be observed that PVA membrane showed clear and homogeneous without bubbles. Whereas HAP agglomerated causing the roughness of PVOH-HAP composites from the addition of HAP from range of 10 % to 30 %. When the HAP increased to 40 %, the HAP could be dispersed well in the PVOH matrix. This indicates that there were formation of hydrogen bonding between HA and PVOH.

For FTIR, the results showed the intensity of absorbance with the increasing loading level of pure materials and composites from range of 500 to 4000 cm^{-1} . Pure PVOH had hydroxyl groups (O-H) at 3341 cm^{-1} , asymmetric and symmetric stretching (-CH₂-) at around 2800 cm^{-1} , O-H and C-H bending at 1400 cm^{-1} and also C-O stretching at 1110 cm^{-1} .

For pure HAP, it had O-H groups at 630 and 3570 cm^{-1} . There were also v₃ and v₄ vibration modes of regular tetrahedral PO₄³⁻ at 1000-1100 cm^{-1} and 560-570 cm^{-1} respectively. The v₁ symmetric stretching of phosphate group was observed at 957 cm^{-1} . The band at 1641 cm^{-1} indicated the presence of H₂O.

For composites, a broad and strong band, O-H stretching frequency at 3360 cm^{-1} determined the presence of HA in composites. There was shifting of band around 3300-3400 cm^{-1} . PVA spectrum at 900 cm^{-1} disappeared, which was caused by the chemical bonding interaction between HAP and PVOH in the nanocomposites. Figure 2.21 and Figure 2.22 show the FTIR spectra of pure PVOH, pure HAP and PVOH-HAP composites.

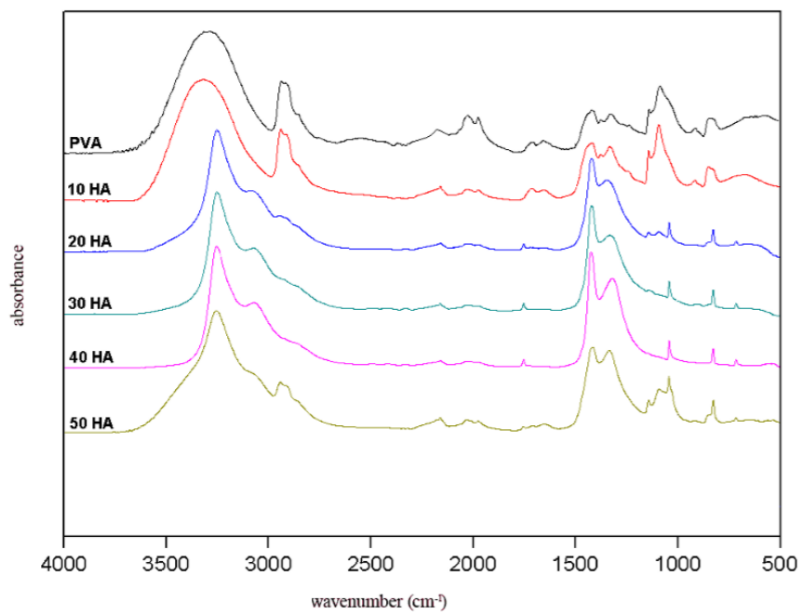


Figure 2.21: FTIR Spectra of Pure PVOH and PVOH-HAP Composites (Balgova et al., 2013).

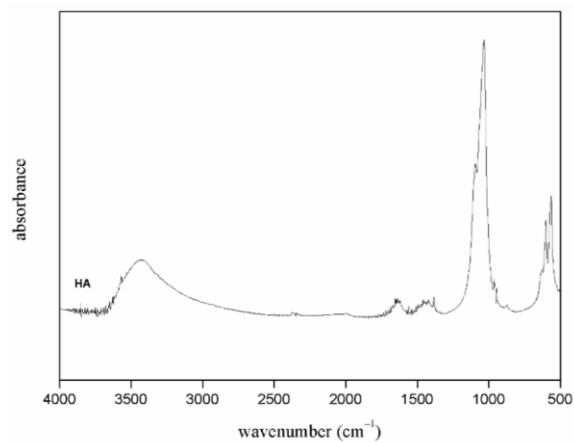


Figure 2.22: FTIR Spectrum of Pure HAP (Balgova et al, 2013).

CHAPTER 3

MATERIALS AND METHODOLOGY

3.1 Materials

Fully hydrolysed polyvinyl alcohol produced by Denki Kougyo Kabushiki Kaisya (DENKI) was used as a polymer in this study.

Nano-size montmorillonite (MMT) clay was purchased from an online supplier. It was used as reinforcing agent in this study. Cuttlebone (*Sepia Officinalis*) was collected from marine sea and purchased from online supplier. As shown in Figure 3.1, cuttlebone was then prepared by calcining at 900 °C for 3 hours.

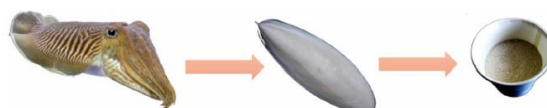


Figure 3.1: Stages of Preparation of Cuttlebone Particles.

3.2 Formulation

There were 6 samples prepared with the variation of MMT and cuttlebone in the constant amount of PVOH as shown in Table 3.1. The amount of PVOH used was fixed at 10g as the basis for other additives. The montmorillonite was varied for 1 phr, 2 phr and 3 phr whereas the cuttlebone varied between 2 phr and 5 phr. Table 3.1 shows the formulation composition needed in casting samples.

Table 3.1: Formulation of PVOH, MMT and Cuttlebone.

Polyvinyl alcohol (phr)	Montmorillonite (phr)	Cuttlebone (phr)
100	1	2
100	2	2
100	3	2
100	1	5
100	2	5
100	3	5

3.3 Sample Preparation

The solution cast samples of PVOH-cuttlebone-MMT were prepared. Firstly, PVOH and MMT were mixed and dissolved in 300 mL of distilled water at 97 ± 2 °C for 30 minutes using a water bath until all the PVOH dissolved. The amount of MMT was varied in 1 phr, 2 phr and 3 phr with 10 g of PVOH. A stirrer was used to stir the mixtures for 1 hour at room temperature. Here suspension solution was formed. As the PVOH complete dissolved in distilled water, additional 100 mL of distilled water was added together with cuttlebone. Cuttlebone was then added with varied amount of 2 phr and 5 phr. Next, the PVOH-cuttlebone-MMT blend was heated again in the water bath at the same temperature, 97 ± 2 °C for 1 hour. The mixture was casted in the form of film in Petri dishes and dried in a vacuum oven at about 65 °C for about 48 hours. Few samples were prepared for each test. After that, the samples were sealed in zig bags and stored at room temperature 25 °C. It has conditioning of 65 % relative humidity.

3.4 Characterisation Test

3.4.1 Tensile Test

Tensile test was conducted using Instron 5582. Mechanical properties such as tensile strength, Young's Modulus and elongation were obtained through tensile test. This test was conducted based on ASTM D 882 standard with rate of 50 mm/min. The samples was situated at the clench of the instrument and aligned in the long axis of the respective specimen. The final value of tensile strength for each sample were measured from the average of 5 specimens.

3.4.2 Scanning Electron Microscopy (SEM) Observation

Surface morphologies of the fractured sample and the microstructure of the film which was incorporated with cuttlebone and MMT were observed. The samples were cut into small portion with length not more than 3 mm. The cut samples were then placed and pasted on the copper stub with the fractured surface facing up. Moreover, these samples were coated with a thin gold layer in order to proceed for scanning. The SEM photographs were observed and recorded under the microscope at magnification of 1000 ×, 1500 × and 2000 ×.

3.4.3 X-ray Diffraction (XRD) Test

The crystallinity structure was observed through XRD test using Shinadzu XRD 6000 diffractometer with Cu-K α radiation ($\lambda = 1.542\text{\AA}$) for a range of scattering angles 2θ ($5^\circ < \theta < 40^\circ$) at a scan rate of $1.2^\circ/\text{min}$. By using 40 kV and 30 mA, the test was implemented with a thin-film attachment that rotated at a fixed speed. The inter-chain separation and d-spacing of PVOH-cuttlebone-MMT were calculated based on the Bragg's formula. The crystallite size, L was calculated using the Scherrer equation as follow:

$$L = \frac{K\lambda}{\beta \cos\theta} \quad (3.1)$$

Samples were cut into 1cm x 1cm x 1cm and prepared in the form of thin films in order to proceed to XRD scanning.

3.4.4 Fourier Transform Infrared Spectrometry (FTIR) Test

The samples were investigated by using ThermoScientific Nicolet iS10 under the range spectrum from 4000 cm^{-1} to 400 cm^{-1} , with accuracy better than $\pm 4\text{ cm}^{-1}$. The samples were be placed on the sample holder before scanning.

3.4.5 Differential Scanning Calorimetry (DSC) Test

DSC analysis was performed using Mettler Toledo DSC823. The samples with a weight of 1-10 mg were determined and loaded into crucible. The scanning was carried out from $30\text{ }^\circ\text{C}$ to $200\text{ }^\circ\text{C}$ at a scanning rate of $10\text{ }^\circ\text{C}/\text{min}$ under dry nitrogen of nearly 100 % purity at a purge rate of $20\text{ mL}/\text{min}$. The DSC thermograms were used to obtain the onset and endpoint melting temperatures for the samples.

CHAPTER 4

RESULTS AND DISCUSSIONS

4.1 Mechanical Properties Analysis

Figure 4.1 shows the mechanical properties of all PVOH-cuttlebone-MMT nanocomposites. Tensile strength, Young's modulus and tensile elongation were determined from the stress-extension curve. The curve is non-linear, where the tangent to the initial stage of the curve gives Young's modulus of blends. Generally, the mechanical properties of composites mainly depend on the dispersion of calcined cuttlebone and MMT with PVOH matrix.

4.1.1 Tensile Strength Test

Based on Figure 4.1(a), various loading level of MMT ranging from 1 phr to 3 phr were added into PVOH with fixed 2 phr and 5 phr of cuttlebone. When different amount of MMT was incorporated with PVOH at fixed 2 phr cuttlebone loading level, the highest tensile strength was observed with value of 41 MPa when 1 phr of MMT were added. The tensile strength then decreased from 41 MPa to 28 MPa, and then increased again to 29 MPa when more than 1 phr of MMT was added. The reduced tensile strength was attributed to the non-homogeneous distribution of MMT on PVOH matrix. Agglomeration of MMT particles occurred causing stress concentration on polymer matrix when subjected to extension. PVOH matrix had poor intercalation effect in MMT galleries. Nevertheless, tensile strength of PVOH-cuttlebone composites increased when the amount of MMT was added to 3 phr. PVOH has extensive amount of hydroxyl functional group that would interact excellently with inherent hydrophilic characteristic of MMT. Hydrogen bonding could be formed to bind MMT strongly with PVOH matrix. High amount of MMT would act as lubricating agent to slide between PVOH-cuttlebone blends. The good intercalation of MMT promoted the effective transfer of extension loading of MMT to silicates.

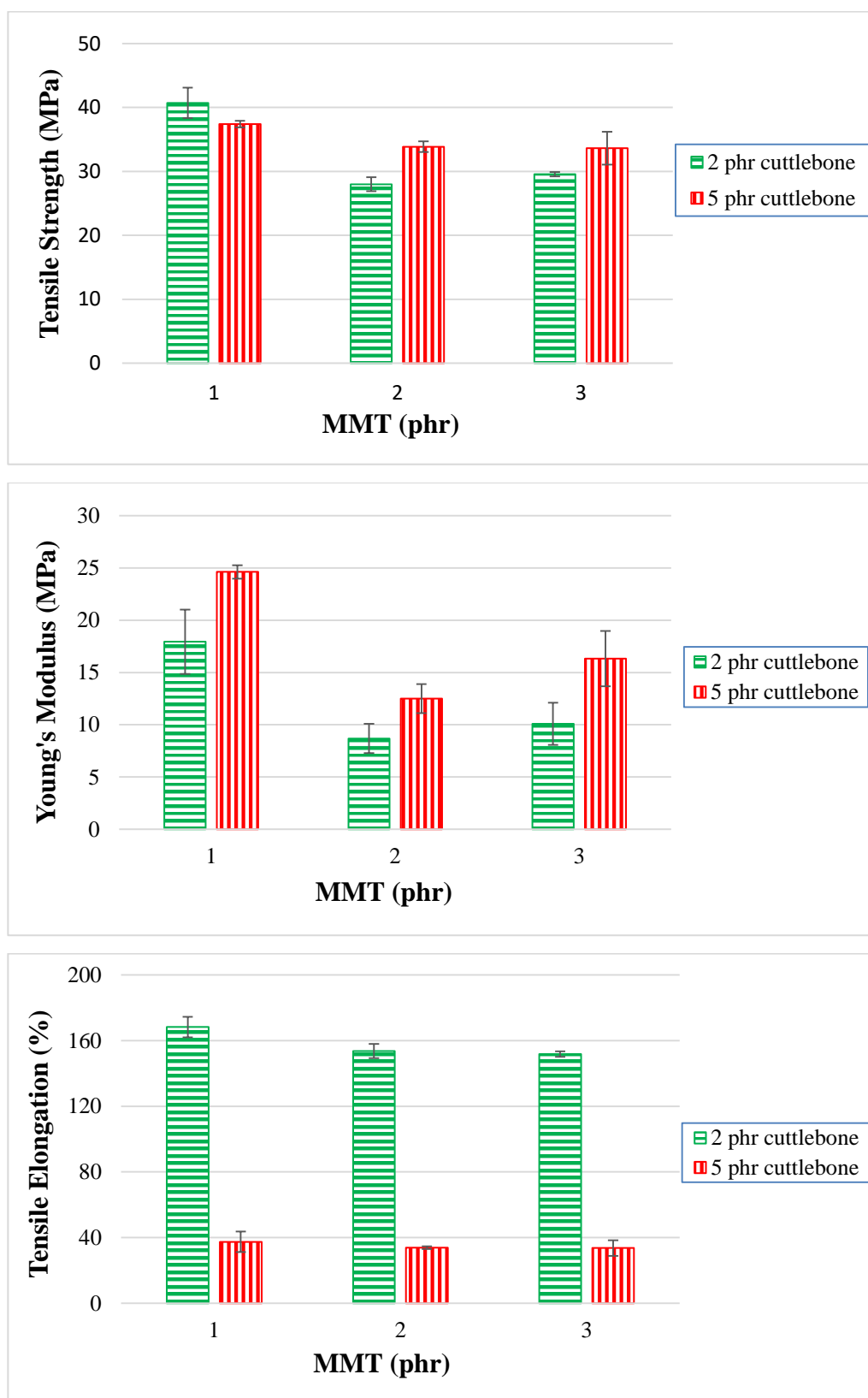


Figure 4.1: (a) Tensile Strength, (b) Young's Modulus and (c) Tensile Elongation (%) for PVOH-cuttlebone-MMT Nanocomposites.

Besides, when the amount of cuttlebone increased to fixed 5 phr loading level, it was found that the tensile strength of PVOH-cuttlebone-MMT nanocomposites decreased gradually. This result was resembled with observation of composites added with varied MMT loading level with fixed 2 phr cuttlebone. This is due to the uneven dispersion of MMT agglomerates causing inferior effect to PVOH matrix. The phase separation ruined the continuity of PVOH matrix and further weakened the mechanical performance of nanocomposites.

On the other hand, Figure 4.1(a) also shows nanocomposites with various amount of cuttlebone incorporated with PVOH with fixed 1 phr, 2 phr and 3 phr of MMT. At fixed low amount 1 phr MMT, as the loading level of cuttlebone increased, the tensile strength decreased. This indicates that cuttlebone was incompatible with MMT and PVOH due to agglomeration of cuttlebone. The cuttlebone tended to form stronger hydrogen bonding within themselves rather than within PVOH matrix. Effective aspect ratio decreased and the agglomerated cuttlebone particles would disturb the regular chain of PVOH. Hence, less energy was required to break the weak intermolecular force, causing the reduction of tensile strength. The cuttlebone was considered to give less reinforcing effect to PVOH matrix.

Furthermore, when the loading level of MMT were fixed at 2 phr and 3 phr, the increasing cuttlebone would increase the tensile strength. Since fillers and PVOH contain hydroxyl groups, cuttlebone formed strong hydrogen bonds with PVOH matrix and MMT, giving good compatibility to composites to bear more stress load in the composites. According to Soltani et al. (2013), cuttlebone have nucleation role that can change crystallographic orientation of nucleation and control its location. This resulted in uniform stress distribution and less void with each other. The enhanced tensile strength was achieved as the agglomeration of cuttlebone could be counterbalanced by addition of high amount of MMT.

4.1.2 Young's Modulus

Figure 4.1 (b) illustrates Young's Modulus of various PVOH-cuttlebone-MMT nanocomposites, showing similar results with the observation

for tensile strength test. When the amount of cuttlebone was fixed at 2 phr with increasing loading level of MMT, there was a drop in Young's Modulus of 50 %, and then went up to 14 %. Young's Modulus declined significantly due to the agglomeration of MMT. There was poor adhesion between the MMT and PVOH-cuttlebone blends as the particles competed with each other to form hydrogen bonds with polymer matrix. Weak interface zone was then generated causing the disintegration of bonds. This resulted in low aspect ratio of MMT, leading to reduced rigidity of polymer blends, elastic deformation was resisted (Barkoula et al., 2008). Furthermore, Young's Modulus increased when the amount of MMT was up to 3 phr. MMT formed firm hydrogen bonds with PVOH matrix which could restrict polymer chain motion. High stress and low strain resulted in high modulus value, causing the composites have high resistant to move. Although MMT and cuttlebone agglomerated together, there was evenly distribution between MMT and PVOH-cuttlebone blends.

When the amount of cuttlebone was fixed at 5 phr, the Young's Modulus of PVOH-cuttlebone-MMT nanocomposites fell gradually from 25 kPa to 13 kPa and further increment up to 16 kPa. One of the noticeable trend is the highest Young's Modulus with the value of $25 \text{ kPa} \pm 0.64$ for 1 phr of MMT and 5 phr cuttlebone incorporated with PVOH. It had the highest rigidity and stiffness which attributed to the nice dispersion between PVOH matrix, MMT and cuttlebone fillers.

Moreover, Figure 4.1(b) also depicts various loading level of cuttlebone, 2 phr and 5 phr were added into PVOH with fixed 1 phr, 2 phr and 3 phr of MMT. The increasing trend happened for all fixed loading level of MMT. Cuttlebone fillers provided significant effect on reinforcement for nanocomposites. There were strong intermolecular and intramolecular hydrogen bonding within nanocomposites. Owing to the properties of high rigidity and stiffness of cuttlebone, the cuttlebone particles interacted and dispersed homogeneously in PVOH matrix, contributing to high Young's Modulus.

4.1.3 Tensile Elongation

Meanwhile, Figure 4.1(c) presents tensile elongation at various loading level of MMT ranging from 1 phr to 3 phr added into PVOH with fixed 2 phr

and 5 phr of cuttlebone. When the cuttlebone was fixed at 2 phr, the tensile elongation decreased gradually, which was caused by the agglomerates by subsequent high loading level of MMT. MMT was unable to distribute evenly in PVOH matrix, eventually the region stress concentration increased in the polymer matrix. Irregular matrix chain was formed as the formed clusters MMT prevented the smooth flow of PVOH. Addition of MMT might increase brittleness of polymer blends, contributing to reduction of ability to deform before fracture. It brought to lower elongation at break as the recrystallization was restricted during deformation. It could be observed that the highest tensile elongation was at 100 phr PVOH-2 phr cuttlebone-1 phr MMT composite due to the high strain at its breaking point. The observation for fixed 5 phr cuttlebone was similar with the previous observation when the cuttlebone was fixed at 2 phr.

This analysis also demonstrates nanocomposites with various amount of cuttlebone incorporated with PVOH with fixed loading level of MMT. The percentage tensile elongation graph shows downward trend for all fixed loading level of MMT. This is because the increasing amount of cuttlebone induced the poor dispersion of cuttlebone particles on PVOH matrix due to the aggregation of cuttlebone particles. More stress concentration region was created along the cuttlebone particles led to the reduction of chain sliding ability. Reinforcing effect of cuttlebone was not significant, the polymer ductility reduced, causing the elongation drop dramatically. Overall, only small amount MMT and cuttlebone fillers showed good reinforcing effect to PVOH matrix as elongation at break obviously exhibits the highest result at the nanocomposite incorporated with PVOH, 1 phr MMT and 2 phr cuttlebone. The polymer chain was pulled with hook of MMT and thus extending the length of PVOH chain, thus increasing the elongation of the composites.

4.2 Scanning Electron Microscopy (SEM)

4.2.1 Interaction of PVOH-Calcined Cuttlebone with Various Amount of MMT

Figure 4.2 and Figure 4.3 show the fracture surface morphologies of all cuttlebone added PVOH nanocomposites at various loading level of MMT. For

all MMT-cuttlebone-PVOH composites at fixed 2 phr cuttlebone, there were formation of fibrils in PVOH matrix due to the resistance ability of matrix from being elongated. The tearing matrix appeared for all varied amounts of MMT in PVOH-cuttlebone composites because of discontinuity matrix form. Besides, when the MMT was at 1 phr, it had the best matrix continuity which indicated homogeneous distribution of MMT particles. MMT formed hydrogen bonding with PVOH matrix contributed to good interfacial adhesion of MMT and thus good dispersion within PVOH matrix. The resistant tearing effect on of PVOH matrix was good by extending the continuity of macromolecules chains. The load was transferred effectively, enabling matrix to elongate more when the stress was applied. The blend was able to break in an ordered way throughout the matrix by producing long fibrils. This is further in agreement with tensile strength results, representing the highest tensile strength and tensile elongation.

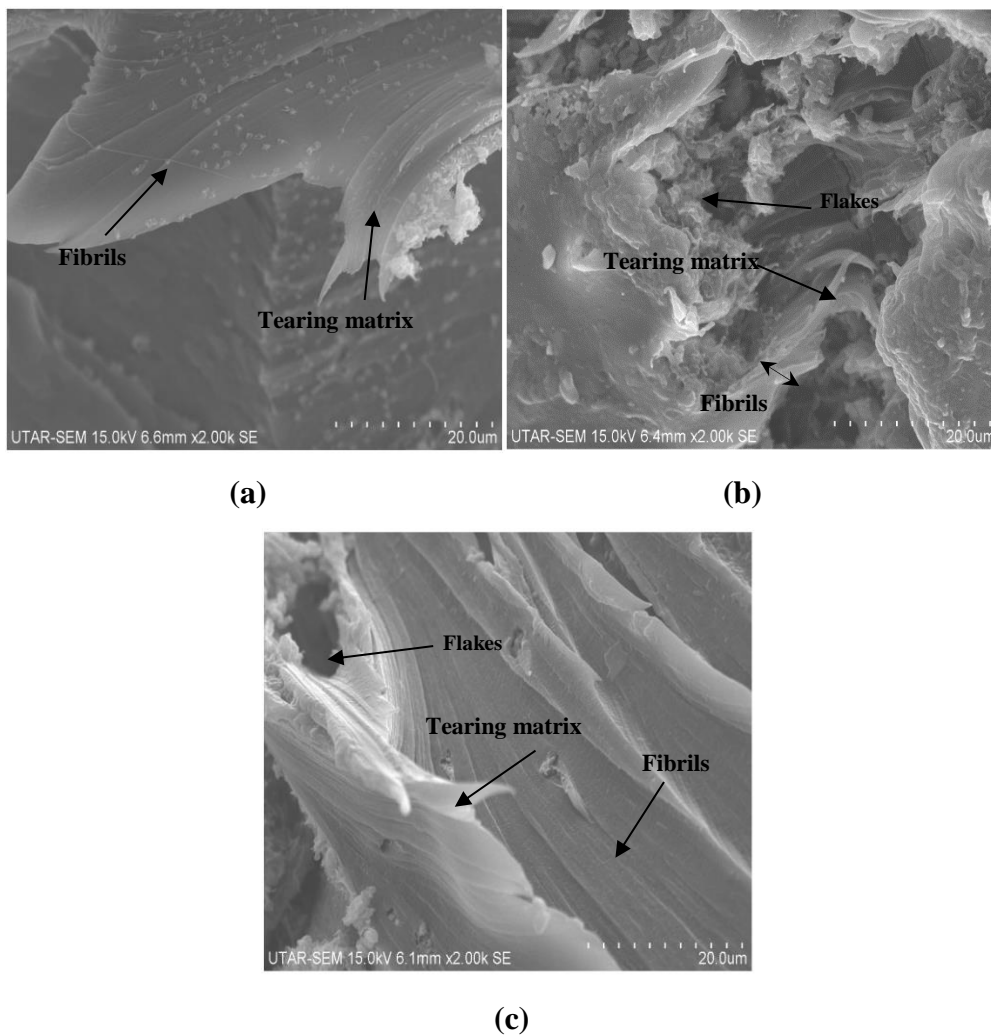


Figure 4.2: SEM of 2 phr Calcined Cuttlebone Incorporated into PVOH Matrix Added with (a) 1 phr MMT (b) 2 phr MMT and (c) 3 phr MMT.

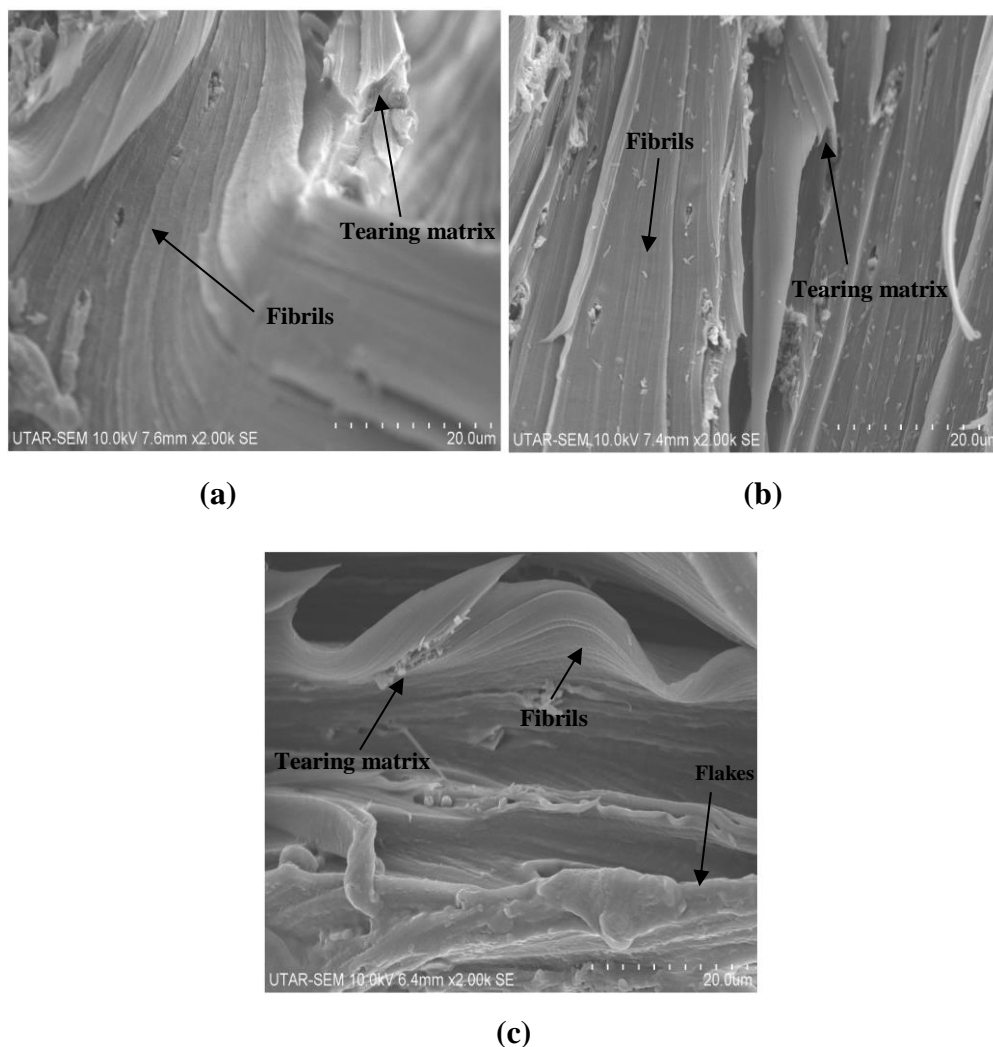


Figure 4.3: SEM of 5 phr Calcined Cuttlebone Incorporated into PVOH Matrix Added with (a) 1 phr MMT (b) 2 phr MMT and (c) 3 phr MMT.

Moreover, by referring Figure 4.2 (b), when the amount of MMT increased to more than 1 phr, the flake-like structures were present on the surface of the nanocomposites. The flake-like structures were seen to increase drastically. This implies that increasing MMT amount could promote the agglomeration effect of MMT in PVOH matrix. Non-homogeneous distribution of MMT particles in PVOH caused by agglomerates also hinders the mobility of slippage in PVOH chains during crystallization. The agglomeration of MMT forms a stress concentration region, contributing to the ineffective transfer of load. Short fibrils were also observed in Figure 4.2 (b). This is further resembled with the decrease in tensile strength and tensile elongation compared to the composite as shown in Figure 4.2 (a).

Moreover, less agglomerates were observed in Figure 4.2 (c), conforming that the tensile strength for 3 phr MMT with PVOH-cuttlebone blends was higher than 2 phr MMT with PVOH-cuttlebone blends. There was only slight aggregation where the effect was not significant. The superior properties overrode the inferior properties, contributing to the good continuity of macromolecules chains.

At fixed 5 phr cuttlebone, when the amount of MMT was at 1 phr, the continuity of matrix was smooth in Figure 4.3 (a). However, when the amount of MMT increased to 2 phr and 3 phr, distinct characteristics of composites such as tearing matrix, flake-like structure and fibrils exhibited on the surface of composites as shown in Figure 4.3 (b) and Figure 4.3 (c). The structures of nanocomposites are slightly changed especially for 3 phr cuttlebone incorporated PVOH-cuttlebone blends. The brittleness effect increased and caused the nanocomposites break faster when high stress was applied. Therefore, they eventually provided low tensile strength and elongation.

4.2.2 Interaction of PVOH-MMT with Various Amount of Calcined Cuttlebone

Figure 4.2 and Figure 4.3 also illustrate the fracture surface morphologies of all MMT added PVOH nanocomposites at various loading level of cuttlebone. For all MMT-cuttlebone-PVOH composites at fixed 1 phr MMT, the surface becomes rough with the increment of calcined cuttlebone as shown in Figure 4.2 (a) and Figure 4.3 (a). Tearing matrix and also fibrils are present in the composites. The agglomeration of cuttlebone could not be counterbalanced by addition of MMT in PVOH matrix. So, as the amount of cuttlebone increased up to 5 phr, agglomeration started to occur where the matrix showed discontinuity. Cuttlebone formed hydrogen bonds within themselves rather than with PVOH matrix. Cuttlebone tended to have phase separation, leading to poor distribution of cuttlebone in PVOH matrix. The matrix continuity reduced causing brittleness of composites. The blend would break faster when stress was applied, further decreasing tensile strength and elongation.

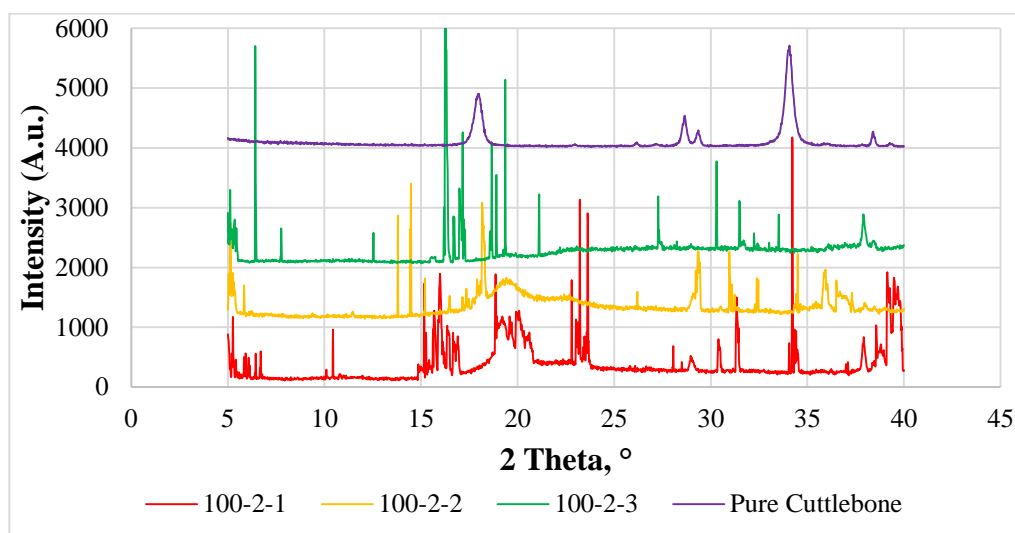
The superior effect was only limited up to certain loading level. It could be seen when the amount of cuttlebone increased to 5 phr with fixed 2 phr and

3 phr MMT in PVOH matrix, the tensile strength increased because of its good reinforcing effect. Less flake-like structure could be observed compared to that 2 phr cuttlebone filled composite. This was attributed by the well dispersion of both agglomerated cuttlebone and MMT, There were strong hydrogen bonding between the blends that could resist tearing effect by developing continuous tearing matrix. However, short fibrils were observed as the elongation decreased. The blends had better tensile strength but poor tensile elongation.

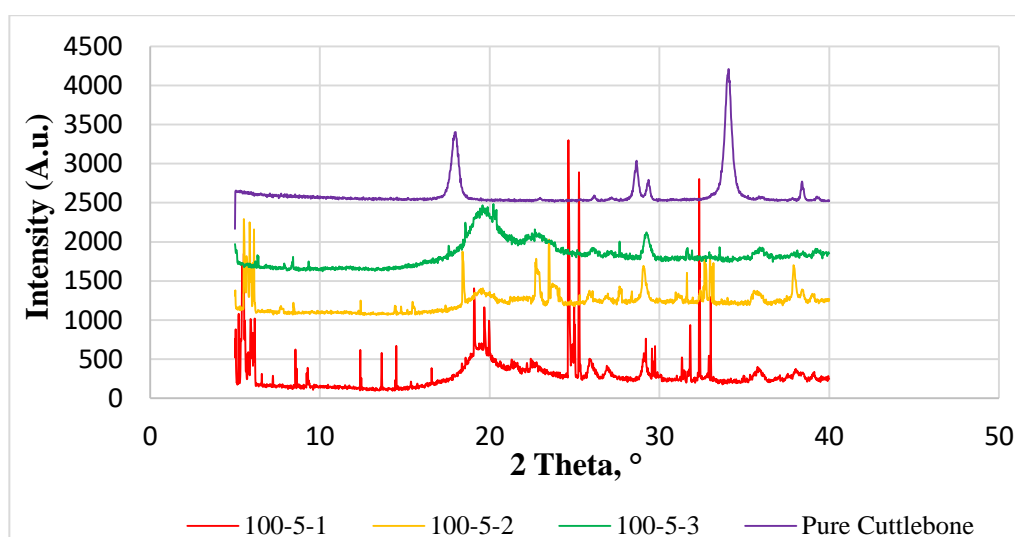
4.3 X-Ray Diffraction (XRD) Test

4.3.1 Description of Peaks

According to Uma Maheshwari et al. (2014), diffraction peak of pure MMT is observed at 7° , 12° , 20° , 21° , 24° , 26° , and 29° whereas the diffraction peaks of calcined cuttlebone are found at 2θ values of 18° , 26° , 28° , 28.7° , 29.4° , and 38.48° respectively as shown in Figure 4.4. Based on Pan and Xiong (2010), an obvious broad peak at 11.4° , 19.5° and 40° corresponds to the characteristics peak of pristine PVOH (Hajeeassa et al., 2018).



(a)



(b)

Figure 4.4: XRD Curves ($5^\circ \leq 2\theta \leq 40^\circ$) for (a) Pure Cuttlebone and PVOH Added with 2 phr of Pure Cuttlebone and Various Loading Level of MMT (b) Pure Cuttlebone and PVOH Added with 5 phr of Pure Cuttlebone and Various Loading Level of MMT.

Besides, Figure 4.4 shows the XRD patterns of varied calcined cuttlebone added polyvinyl alcohol nanocomposites with fixed amount of montmorillonite from $2\theta = 5^\circ$ to $2\theta = 40^\circ$. Based on Wei, Song and Zhang (2014), the broad peak at $2\theta = 19.4^\circ$ assigned to (101) was caused by the diffraction of the crystal plane of PVOH, which was due to the intermolecular

hydrogen bonding between PVOH chains. This XRD pattern demonstrates its semi-crystalline structure because it has high affinity to form hydrogen bonds.

Overall, when the higher amount of cuttlebone fillers were embedded into PVOH matrix, they were well dispersed until the crystallite structure disappeared. Cuttlebone have clear crystals which undergo random crystallisation after adding into matrix. PVOH disturbed the highly ordered structure of cuttlebone, causing disappearance of deflection peaks at 18° , 26° , and 28° . The molecules were changed due to phase separation of composites, leading to good interaction with PVOH chains. Furthermore, it could be seen that MMT posed insignificant effect to the interaction with the PVOH matrix due to the presence of MMT deflection peaks. Poor dispersion of MMT in PVOH matrix resulted in agglomeration of MMT particles when MMT was incorporated with PVOH matrix. Hence, formation of crystallite structure was induced by organic MMT, eventually generating most of sharp crystallite peaks on XRD curves.

4.3.2 Crystallite size and d-Spacing of All PVOH - Cuttlebone - MMT Composites

Table 4.1 presents the crystallite size and d-spacing at $2\theta = 19.4^\circ$ for all PVOH-cuttlebone-MMT composites. At fixed 2 phr cuttlebone loading level, it can be observed that addition of MMT loading level could lower the intercalation effect of MMT in PVOH matrix by referring to decrement of d-spacing due to agglomeration of MMT particles. The crystallite size also decreased from 611.41 \AA to 84.86 \AA and then increased to 611.05 \AA as shown in Table 4.1. MMT particles were separated from PVOH-cuttlebone phase. Decrement of d-spacing will increase the compactness on this deflection peak. The d-spacing of polymer composites was directly related to the tensile strength of composites. This implies that when the d-spacing decreased, the tensile strength of polymer composites decreased.

Table 4.1: d-Spacing and Crystallite Size at $2\theta = 19.4^\circ$ for All PVOH-Cuttlebone-MMT Composites.

Loading level of cuttlebone (phr)	Loading level of MMT (phr)	d-spacing, d (Å)	Crystallite size, L (Å)
2	1	4.58116	611.41
2	2	4.56907	84.86
2	3	4.46249	611.05
5	1	-	-
5	2	-	-
5	3	4.50829	41.61

However based on Table 4.1, 100 phr PVOH-5 phr cuttlebone-1 phr MMT and 100 phr PVOH – 5 phr cuttlebone – 2phr MMT had no signature peak at 19.4° , representing that the cuttlebone and MMT interacted well with PVOH matrix, producing random chains in the composites.

4.3.3 Crystallinity

Figure 4.4 (a) displays XRD curves for PVOH blends incorporated with 2 phr cuttlebone and various amount of MMT whereas Figure 4.4 (b) illustrates XRD curves for PVOH blends incorporated with 5 phr cuttlebone and various amount of MMT. Besides, the effect of various MMT and cuttlebone loading level on crystallinity of PVOH nanocomposites is showed in Figure 4.5.

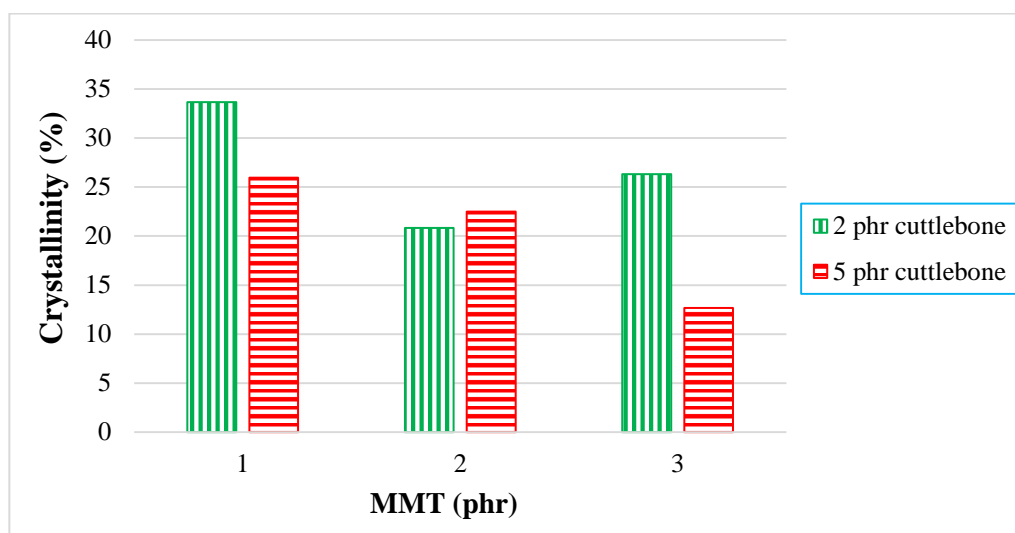


Figure 4.5: Crystallinity of All PVOH-Cuttlebone-MMT Composites.

According to Figure 4.4(a) and Figure 4.4(b), when the loading level of MMT increased, subsequently decreasing the crystallite peaks. This is because high amount of MMT disturbed the formation of highly ordered crystal structure. Based on Figure 4.5, for 2 phr of cuttlebone loading, the crystallinity of composites was slightly decreased from 33.65 % to 20.82 % and then increased to 26.33 % when the various loading level of MMT was added into PVOH matrix. The decrement identifies the addition of MMT would slightly disturb the arrangement of crystal structure in PVOH matrix. It could rupture the orientation of crystalline structure in polymer matrix of PVOH composites. There was non-homogeneous distribution of MMT which avoids the MMT particles from getting into the PVOH-cuttlebone blends. The regularity of matrix chain arrangement was reduced, which resulted in transformation of structure from crystallite to amorphous and thus reduced the crystallinity. Meanwhile, the increased crystallinity exhibited good interaction with polymer matrix, inducing the formation of more crystallite structure. This is because calcined cuttlebone or MMT have hydrophilic characteristic which contains formed hydroxyl groups. They tended to form new hydrogen bonding with polymer matrix, inducing the formation of new crystallites which resulted in an order chain arrangement. These results were in agreement with the tensile strength test.

Furthermore, when the loading level of cuttlebone increased, the crystallite structure decreased, the crystallinity decreased. Agglomeration of cuttlebone in PVOH matrix happened, causing the decrease of interfacial adhesion. No new bond or crystalline structure would be formed. It could be observed that the mechanisms for addition of MMT and cuttlebone on polymer blends are analogous, leading to similar trends for d-spacing as well as the tensile strength test.

4.4 Fourier Transform Infrared (FTIR) Test

4.4.1 FTIR for All PVOH-Cuttlebone-MMT Nanocomposites

Figure 4.6 and Figure 4.7 show infrared spectrum of PVOH-MMT nanocomposites with different loading level of calcined cuttlebone. These FTIR characteristics of PVOH-calcined cuttlebone-MMT exhibit the combined bands of calcined cuttlebone and PVOH. Meanwhile, Table 4.2 depicts the wavenumbers of O-H stretching, C-H stretching and C-O stretching for all PVOH-calcined cuttlebone-MMT nanocomposites.

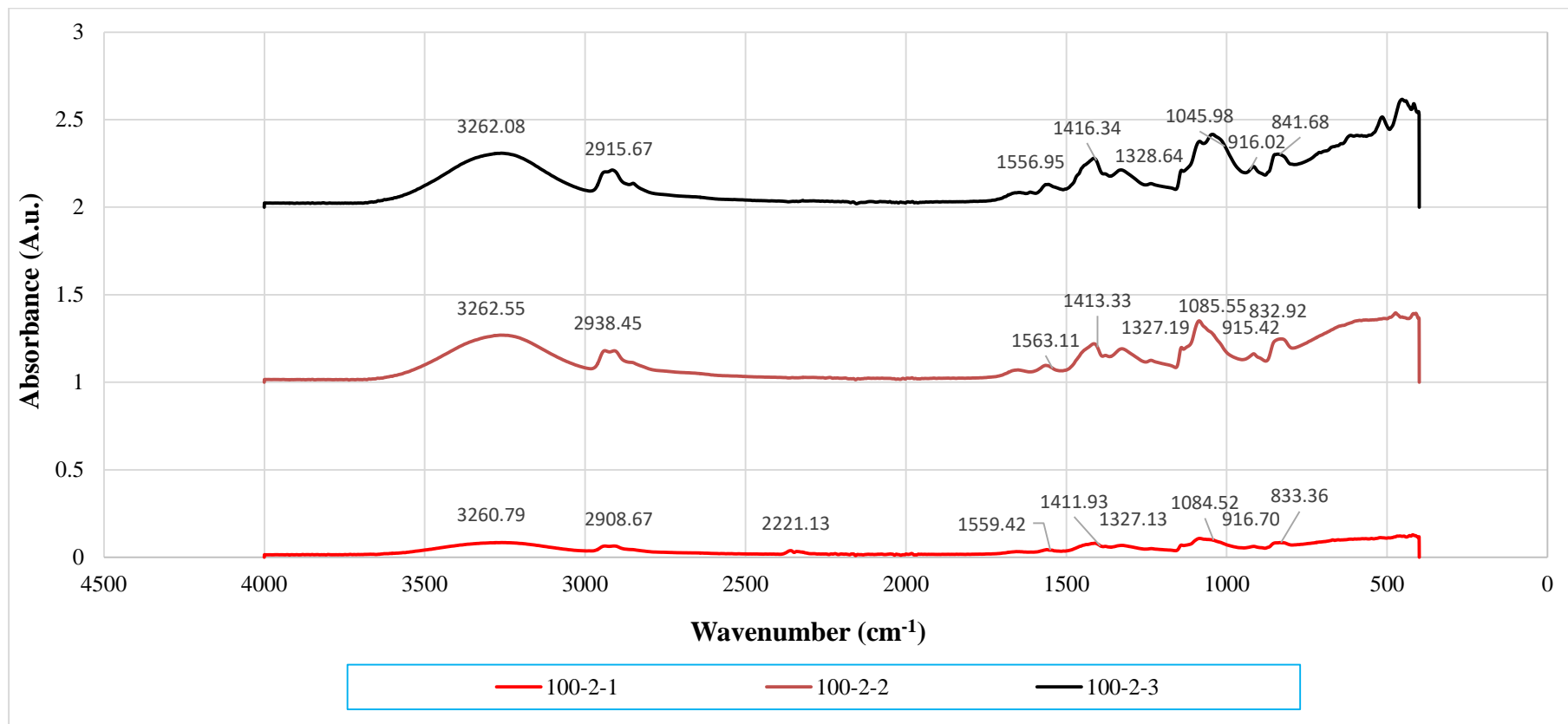


Figure 4.6: Infrared Spectrum of all PVOH-MMT Nanocomposites Added with 2 phr of Calcined Cuttlebone.

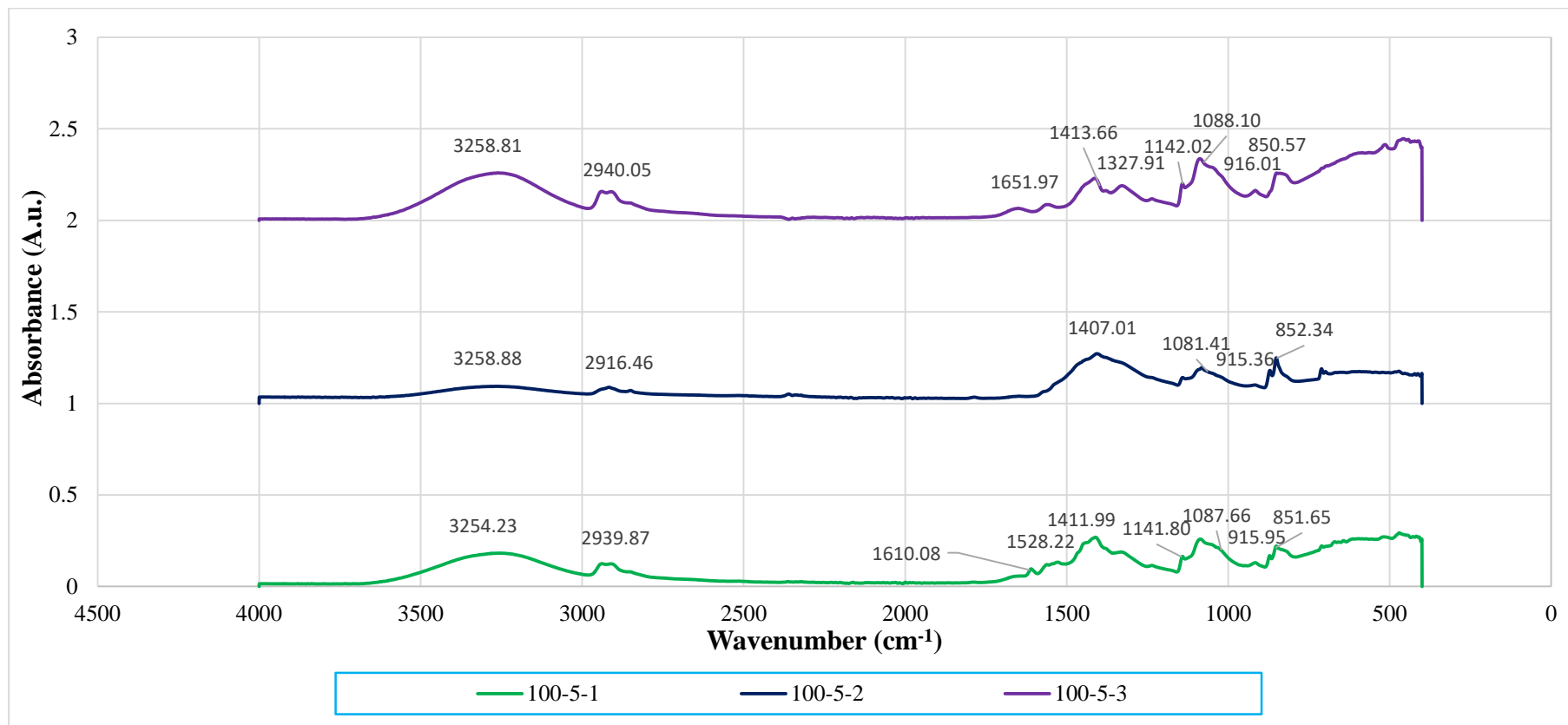


Figure 4.7: Infrared Spectrum of all PVOH-MMT Nanocomposites Added with 5 phr Calcined Cuttlebone.

Table 4.2: Wavenumbers of its Stretching Type for All PVOH-Calcined Cuttlebone-MMT Nanocomposites.

Loading level of MMT (phr)	Loading level of calcined cuttlebone (phr)	Wavenumber (cm ⁻¹)		
		O-H stretching	C-H stretching	C-O stretching
1	2	3260.79	2908.67	1084.52
2	2	3262.55	2938.45	1085.55
3	2	3262.08	2915.67	1045.98
1	5	3254.23	2939.87	1087.66
2	5	3258.88	2916.46	1081.41
3	5	3258.81	2940.05	1088.10

Based on Figure 4.6, Figure 4.7 and Table 4.2, the most important peak of 3254.23-3262.55 cm⁻¹ represents stretching of hydroxyl functional group. This broad and significant peak was analysed to identify the extent of hydrogen bonding interaction of the composites. There were also several peaks visible, which were C-H functional group in the region of 2908.67-2940.05 cm⁻¹ and C-O stretching in the range of 1045.98-1088.10 cm⁻¹. There were some functional groups that do not participated significantly in the interaction. Hydroxyl bending were found at the wavenumber range of 1407.01-1416.34 cm⁻¹. C-H bending could be observed at the range of 1327.13-1328.64 cm⁻¹ and vibration of carbonate group (CO_3^{2-}) could be observed at the range of 832.92 - 852.34 cm⁻¹.

According to Lim (2018), pure PVOH has vibration of hydroxyl group at around 3282.82 cm⁻¹. Compared with pristine PVOH, the shifting of band position of stretching vibration of hydroxyl groups of all PVOH-cuttlebone-MMT composites to low frequency was induced by red shift effect of hydrogen bonding action, indicating the formation of strong hydrogen bonding between PVOH, MMT and cuttlebone (Guo et al., 2018). This is because PVOH is hydrophilic whereas cuttlebone and MMT has hydroxyl groups on the surface, reducing the hydrophilic nature of PVOH. Interlayer gallery of MMT enabled

the intercalation of polymer chains and cuttlebone to strengthen its interaction. As a result, internal hydrogen bonding between polymer chains in PVOH matrix had been weakened due to the well dispersion and interaction of MMT and cuttlebone in the PVOH matrix, producing synergistic effect (Tee et al., 2013).

At fixed 2 phr and 5 phr cuttlebone, when the MMT loading level increased to 2 phr, the hydroxyl groups had shifted to higher wavenumber. This denotes the decrease of hydrogen bonding with PVOH matrix. Addition of calcined cuttlebone and MMT did not disturb the presence of hydrogen bonding in PVOH matrix. They tended to agglomerate together, causing poor dispersion of both fillers in PVOH matrix. This observation was in agreement with the tensile strength results that increasing amount of MMT could introduce agglomeration (Jiang, Rui and Chen, 2009). In other word, the aggregated MMT and cuttlebone particles had significantly weakened the interaction effect between fillers and PVOH matrix and thus promoted the hydrogen bonds within PVOH matrix itself. But there was a subsequent reduction of wavenumber of PVOH-cuttlebone-MMT composites when it was achieved at 3 phr MMT amount. This indicates the formation of more hydrogen bonds, inducing exfoliation and intercalation effects of MMT to improve the tensile strength of the composites. It notes that extra energy was required to convert into kinetic to generate vibrational effect of composites.

In order to further investigating effect of varied cuttlebone added PVOH-MMT blends, when the cuttlebone increased to 5 phr for all fixed MMT amount, wavenumber of composites was lower compared with 2 phr cuttlebone. It can be obviously noticed that the dominant of cuttlebone had ruined the chain arrangement in the PVOH matrix. Such synergistic interaction of cuttlebone and PVOH-MMT blends could be detected. Thus, it was believed that the enhancement of tensile strength also contributed by the addition of low amount of 1 phr hydrophilic MMT whereby strong secondary hydrogen bonding was formed to provide additional reinforcing interaction among components in the blends. This could be shown as the wavenumber of the O-H functional group is the lowest, which is 3254.23 cm^{-1} .

Besides, wavenumber of C-H and C-O stretching was decreased when rose up to 2 phr MMT and then increased in relation to 3 phr MMT. The

reduction of wavenumber of C-H and C-O stretching indicates the addition of MMT particles can enhance the strength of C-H and C-O bonding inside PVOH matrix by strengthening the structure of PVOH. Thus, the addition of MMT has significantly improved the mechanical properties of composites such as tensile strength. Meanwhile, higher energy was required to overcome the effect caused by the high stiffness of molecular structure when there was the shifting of wavenumber to high frequency.

4.5 Differential Scanning Calorimetry (DSC) Test

Differential scanning calorimetry (DSC) thermogram of PVOH-Cuttlebone-MMT is shown in Figure 4.8. An obvious endothermic peak could be observed at the region of 200 to 250 °C. Besides, the extent melting state of the DSC is also a vital element to express the magnitude of intermolecular bonding in the blends. If there is large peak area or high enthalpy of melting, more thermal energy is needed to convert into kinetic energy to allow the polymer molecules free out from the ordered crystalline structure.

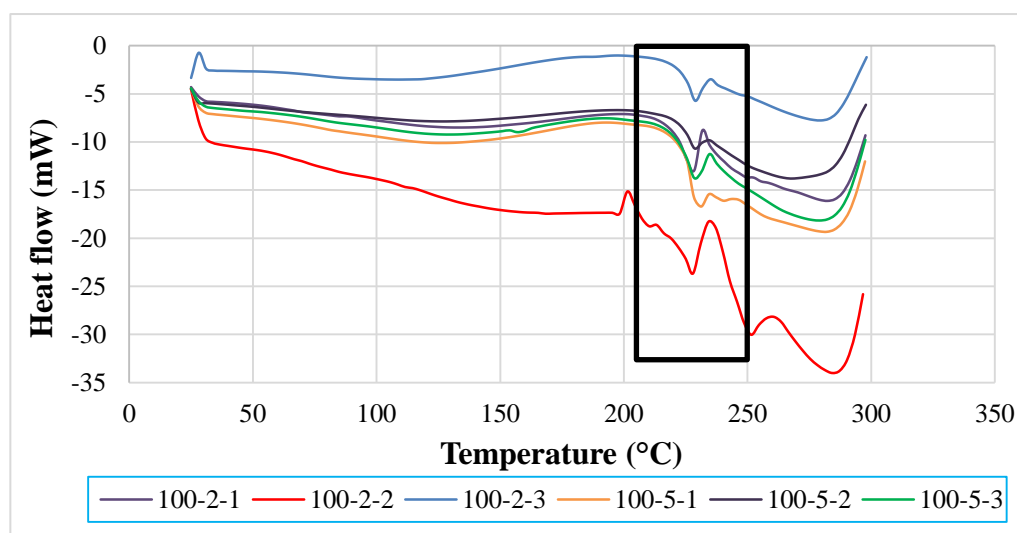


Figure 4.8: DSC Thermogram of PVOH-Cuttlebone-MMT Composites.

4.5.1 Melting Temperature

Melting peaks for all the composites are exhibited in Figure 4.9. At fixed 2 phr cuttlebone, MMT amount was added from 1 phr to 2 phr, the melting temperature decreased. This is because MMT interrupted the interaction of

cuttlebone and polymer matrix, forming larger number of particles with higher size irregularity, promoting occurrence of agglomeration. The chain arrangement of polymer matrix was disrupted, causing non-homogeneous dispersion of MMT on PVOH-cuttlebone polymer blends. When MMT amount then increased from 2 phr to 3 phr, the melting temperature increased. MMT acts as an enhancement phase to form secondary bonding. There was good interaction of cuttlebone and MMT with PVOH matrix towards highly stable structure. Cuttlebone and MMT have hydrogen bonds formed with PVOH matrix. At the same time, rigidity increased and more heat energy was needed to vibrate the stronger hydrogen bonding.

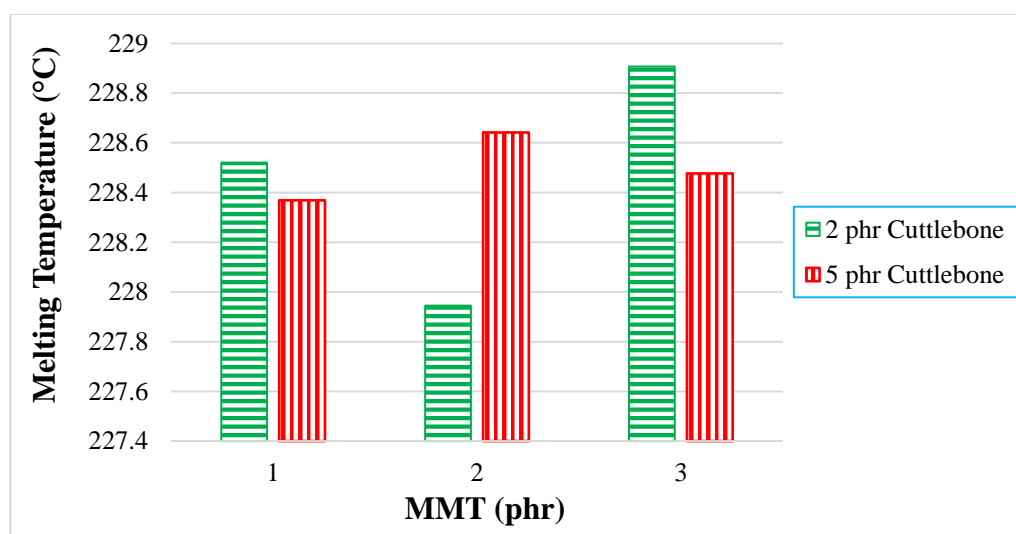


Figure 4.9: Effect of Increasing MMT and Cuttlebone Loading Level on Melting Temperature.

On the other perspective, when the increment of cuttlebone loading level to 5 phr with fixed 1 phr and 3 phr MMT loading level, the melting temperature decreased. There was agglomeration of cuttlebone which relates to uneven distribution of the composites. Interfacial adhesion was weakened thus formation of weaker internal hydrogen bonding of PVOH. It will cause irregular chain arrangement of PVOH matrix that reduces the existing hydrogen bonding strength within polymer matrix. It is further supported by the decreasing tensile strength results. Meanwhile, when the cuttlebone loading level increased to 5

phr and the amount of MMT was fixed at 2 phr, thermal stability was enhanced due to the increasing cuttlebone content. This was attributed to the high rigidity and strength of polymer nanocomposites which was caused by hydrogen bond in cuttlebone inhibited the mobility of chain, eventually effectively improved the melting temperature (Xue et al., 2018). This results are in agreement with FTIR observation where the O-H stretching had shifted to lower wavenumber when there was an increase for cuttlebone loading level. The wavenumber of O-H stretching also has the similar trend with the tensile strength results with increasing of MMT amount. It means that high concentration of cuttlebone and MMT at the same time could be distributed on every corners, forming strong PVOH-cuttlebone-MMT although the agglomeration still occurs. The superior effect of forming large number of hydrogen bonding might dominant over the inferior effect of agglomeration of cuttlebone. Nevertheless, addition of MMT had compensated such inferior effects of cuttlebone in the blends (Tee et al., 2013).

4.5.2 Enthalpy of Melting

For quantitative analysis, the enthalpy of melting (ΔH_M) extracted from the data are tabulated and plotted in Figure 4.10. When there was the increment of MMT from 1 phr to 2 phr for all fixed loading level of cuttlebone, enthalpy of melting decreased. This is because the interaction effect of MMT and polymer matrix reduced. The crystalline structure was disrupted, characterised by the decrement of crystallinity. Whereas when there was increasing of amount of MMT from 2 phr to 3 phr for fixed 2 and 5 phr loading level of cuttlebone, enthalpy of melting increased. Inorganic layers of MMT have promoted a new crystal structure leading to increase of thermal properties. The stiffening behaviour of MMT also improved the crystallinity of PVOH-cuttlebone-MMT nanocomposites. It tended to enlarge the reinforcing effect through physical interaction such as intercalation and exfoliation effects to boost the mechanical strength (Tee, 2013). The interaction of MMT and cuttlebone became intense when blended with PVOH. Addition of MMT at higher amount helped to recover the strong interaction in PVOH-cuttlebone blends. Both reinforcing fillers were well dispersed in PVOH matrix. Similarly, this is evidently shown that the tensile

strength for PVOH blends with 3 phr MMT and 2 phr cuttlebone are higher than that PVOH blends with 2 phr MMT and 2 phr cuttlebone. Besides, according to Young's Modulus data, PVOH blends with 3 phr MMT and 2 phr cuttlebone has higher rigidity with increment of 16.24 % when compared with PVOH blends with 2 phr MMT and 2 phr cuttlebone.

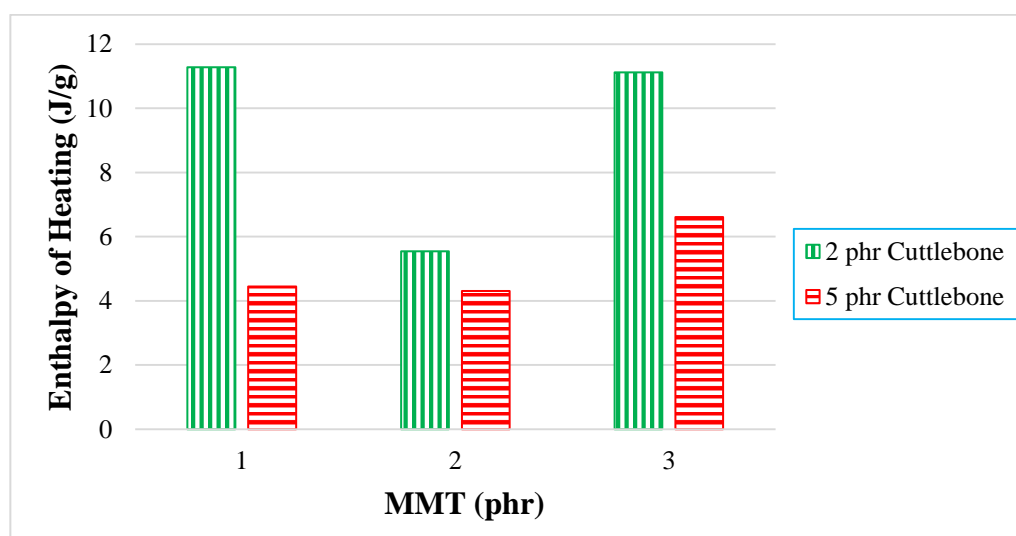


Figure 4.10: Effect of Increasing MMT and Cuttlebone Loading Level on Enthalpy of Melting.

Further examination when there was increasing of cuttlebone from 2 phr to 5 phr incorporated for all fixed loading level of MMT, enthalpy of melting decreased. Addition of cuttlebone in the PVOH had caused significant reduction of enthalpy of heating due to weakening structure of cuttlebone which ruined the intermolecular bonding beyond expectation. Irregularity of cuttlebone caused the inferiority (Tee et al., 2013), limiting the formation of primary bonding. The crystallinity was suppressed by the introduction of cuttlebone into the PVOH matrix. The cuttlebone interaction did not significantly involve in the chemical bonding, like Van der Waals or hydrogen bonding. Lastly, Table 4.3 shows the melting temperature, onset temperature and end temperature for all PVOH-cuttlebone-MMT composites. As noticed for the onset temperature for all samples, with the increment of cuttlebone to 5 phr loading level, it had shifted to higher temperature for each fixed amount of MMT. This is due to induction of pronounce effect with the addition of both MMT and cuttlebone, giving

improvement in thermal stability, which resulted in outstanding blending materials.

Table 4.3: Melting Temperature, Onset and End Temperature of PVOH-Cuttlebone-MMT Nanocomposites.

Loading Level of MMT (phr)	Loading Level of Cuttlebone (phr)	Melting Temperature (°C)	Onset Temperature (°C)	End Temperature (°C)
1	2	228.521	216.778	231.714
2	2	227.945	213.238	234.226
3	2	228.907	216.446	235.017
1	5	228.369	222.654	234.380
2	5	228.642	217.772	234.575
3	5	228.477	216.755	234.606

CHAPTER 5

CONCLUSION AND RECCOMENDATION

5.1 Conclusion

This study was focus on the investigation of Polyvinyl Alcohol (PVOH) blended with calcined cuttlebone and Montmorillonite (MMT). When 5 phr of cuttlebone were added to PVOH-MMT blends at fixed 1 phr MMT, the poor distribution of high amount of cuttlebone particles reduced the tensile strength of the composites. Stress concentration spot was formed subsequently weaken the functionality of physical structure. Nevertheless, such inferior effect was not examined when cuttlebone was added in PVOH-MMT blends with fixed 2 phr and 3 phr MMT, where the tensile strength increased indicating the superior interaction present in this PVOH-cuttlebone-MMT compound. The cuttlebone portion in PVOH-MMT blends would undergo nucleation thus promoting the uniform distribution of cuttlebone particles. When the loading level of cuttlebone increased, Young's Modulus of all composites showed the larger value which is probably attributed to the high rigidity and stiffness of cuttlebone due to the strong intermolecular and intramolecular hydrogen bonding within the nanocomposites. In addition, the elongation of composites with fixed loading of MMT were decreased when subjected to higher 5 phr of cuttlebone loading. This is because the aggregation of cuttlebone particles contributed insignificant reinforcing effect, which are caused by the stress concentration region thus resulting in the reduction of chain sliding ability. The effect of calcined cuttlebone and MMT in PVOH-cuttlebone-MMT composites could be observed via SEM micrograph of fracture surface. The morphology of PVOH-cuttlebone-MMT composites with higher loading level of cuttlebone was seen to have more tearing matrix and fibrils than lower loading level of cuttlebone at fixed 1 phr MMT. Agglomeration was observed where the matrix showed discontinuity, causing the brittleness of composites. The tensile stress and elongation were further decreased. On the other hand, when MMT concentration is high (2 phr and 3 phr), the intercalation effect of cuttlebone is visible. Short fibril and less flake-like structure could be observed in 5 phr cuttlebone

compared to 2 phr cuttlebone due to the well dispersion of cuttlebone and MMT in composites, contributing to the enhanced tensile strength and poor elongation.

XRD analysis confirmed that in overall the cuttlebone were well dispersed until the crystallite structure disappeared. PVOH disturbed the highly ordered structure of cuttlebone, causing the disappearance of deflection peak. Besides, MMT was poor dispersed in PVOH matrix due to agglomeration of MMT. Crystallite structures were formed by the induction of MMT. When the loading level of cuttlebone increased, the crystallite structure decreased, the crystallinity also decreased. The d-spacing also decreased due to low interfacial adhesion of cuttlebone, which is in agreement with tensile strength test. The addition of cuttlebone in pure PVOH has shown red shift effect implying the formation of hydrogen bonding induced by cuttlebone. For FTIR analysis, it was also found that wavenumber of O-H stretching for the composites with all fixed amount of MMT decreased gradually with the increment of cuttlebone. The cuttlebone ruined the arrangement in PVOH matrix and induced the formation of hydrogen bonds to provide the additional reinforcing interaction between components in the blends. When investigation expanded to C-H and O-H stretching, it could be noticed that the wavenumber decreased and then increased in relation to the amount of MMT, which is in agreement with tensile strength test. The increment was induced by the higher stiffness of the molecular structure, enabling the vibrational effect of C-H and C-O infrared absorption. Meanwhile for DSC analysis, by comparing PVOH-MMT added 2 and 5 phr of cuttlebone at fixed 1 phr and 3 phr MMT, the melting temperature decreased due to the agglomeration of cuttlebone, weakening the formation of internal hydrogen bonding. Meanwhile by comparing PVOH-MMT added 2 and 5 phr of cuttlebone at fixed 2 phr MMT, the melting temperature increased. The high concentration of cuttlebone and MMT are distributed evenly in PVOH matrix, forming strong hydrogen bonding. Also, it showed that the melting area was lower at higher loading level of cuttlebone. This exhibited that cuttlebone was irregular, deteriorating the intermolecular bonding beyond expectation. Besides, as noticed for the increment of cuttlebone loading, the onset temperature increased due to the reinforcing effect of cuttlebone and MMT to provide good thermal stability.

5.2 Recommendation for Future Work

It is recommended that more tests should be carried out to determine the properties of the PVOH-cuttlebone-MMT composites. Thermogravimetric analysis (TGA) should be suggested to analyse the thermal stability of nanocomposites. Besides, the overall properties are dependent on the dispersion rate of fillers particles on PVOH matrix. Hence, synthesis process of polymer nanocomposites is crucial to obtain even distribution of fillers on PVOH matrix. The pure cuttlebone materials should be calcined completely with higher temperature to reduce impurities of the samples. In order to produce stronger matrix dispersion, in-situ polymerisation method might be applied to replace the solution casting method. When conducting the casting of the composites, stirring and heating of solution should be maintained at same rate to prevent non-homogeneous dispersion of the samples and bubbles formed. The solution in petri dish should be placed in even surface of oven. Besides, the oven temperature and time keep fluctuating when drying of the samples. Hence, the drying time and temperature should be consistent. When the casted samples are completed, the samples should be placed in zig bag to prevent oxidation of samples. Lastly, the test could be repeated twice to get accurate results.

REFERENCES

- Allison, P.G., Moser, R.D., Chandler, M.Q., Caminero-Rodriguez, J.A., Torres-Cancel, K., Rivera, O.G., Goodwin, J.R., Gore, E.R. and Weiss, C.A. , 2015. Mechanical, thermal, and microstructural analysis of polyvinyl alcohol (PVA)/montmorillonite (MMT) nanocomposites. *Journal of Nanomaterials*, [e-journal] 2015(8), pp.9. <http://dx.doi.org/10.1155/2015/291248>.
- Andreas, A.S., Fotios, K.K. and Nick, K.K., 2011. *Nanocomposites and Polymers with Analytical Methods*. Croatia: InTech.
- Ashwin, K., Karthick, K. and Arumugam, K.P., 2011. Applications_Biodegradable_Materials. *Biochemistry and Bioinformatics*, 1(3), pp.1–4.
- Balgova, Z., Palou, M., Wasserbauer, J. and Kozankova, J, 2013. Synthesis of polyvinyl alcohol-hydroxyapatite composites and Characterisation of their Bioactivity. *Central European Journal of Chemistry*, 11(9), pp. 1403-1411.
- Barkoula, N.M., Alcock, B., Cabrera, N.O. and Peijs, T., 2008. Flame-Retardancy Properties of Intumescent Ammonium Poly(Phosphate) and Mineral Filler Magnesium Hydroxide in Combination with Graphene. *Polymers and Polymer Composites*, [e-journal] 16(2), pp.101–113. <https://doi.org/10.3390/polym6112875>
- Bee, S.T., Ratnam, C.T., Lee, T.S., Tee, T.T., David, H., Kadhum, A.A.H., Rahmat, A.R. and Joshin, L., 2014. Effects of electron beam irradiation on mechanical properties and nanostructural-morphology of montmorillonite added polyvinyl alcohol composite. *Composites Part B: Engineering*, [e-journal] 63 (2014), pp.141–153. <http://dx.doi.org/10.1016/j.compositesb.2014.03.021>
- Birchall, J.D. and Thomas, N.L., 1983. On the architecture and function of cuttlefish bone. *Journal of Materials Science*, 18(7), pp.2081–2086.
- Cadman, J., Zhou, S., Chen, Y. and Li, Q., 2012. Cuttlebone: Characterisation, Application and Development of Biomimetic Materials. *Journal of Bionic Engineering*, [e-journal] 9(3), pp.367–376. [http://dx.doi.org/10.1016/S1672-6529\(11\)60132-7](http://dx.doi.org/10.1016/S1672-6529(11)60132-7)
- Darder, M., Colilla, M. and Ruiz-Hitzky, E., 2003. Biopolymer-clay nanocomposites based on chitosan intercalated in montmorillonite. *Chemistry of Materials*, 15(20), pp.3774–3780.
- Elbadawy, K., Mohamed Elsayed, Y., Alaa, F. and Hazem Fathallah, K., 2015. Ion conducting nanocomposite membranes based on PVA-HA-HAP for fuel cell application: II. Effect of modifier agent of PVA on membrane properties. *International Journal of Electrochemical Science*, 10(8), pp.6627–6644.

Faksawat, K., Sujinnapram, S., Limsuwan, P., Hoonnivathana, E. and Naemchanthar, a K., 2015. Preparation and Characteristic of Hydroxyapatite Synthesized from Cuttlefish Bone by Precipitation Method. *Advanced Materials Research*, 1125 (5), pp.421–425.

Ferro, A.C. and Guedes, M., 2019. Mechanochemical synthesis of hydroxyapatite using cuttlefish bone and chicken eggshell as calcium precursors. *Materials Science and Engineering C*, 97, pp.124–140. <https://doi.org/10.1016/j.msec.2018.11.083>.

Florek, M., Fornal, E., Gomez-Romero, P., Zieba, E., Paszkowicz, W., Lekki, J., Nowak, J. and Kuczumow, A., 2009a. Complementary microstructural and chemical analyses of *Sepia officinalis* endoskeleton. *Materials Science and Engineering C*, [e-journal] 29(4), pp.1220–1226. <http://dx.doi.org/10.1016/j.msec.2008.09.040>.

Gaaz, T.S., Sulong, A.B., Akhtar, M.N., Kadhum, A.A., Mohamad, A.B. and Al-Amiert, A.A., 2015. Properties and applications of polyvinyl alcohol, halloysite nanotubes and their nanocomposites. *Molecules*, 20(12), pp.22833–22847.

Gaidukov, S., Danilenko, I. and Gaidukova, G., 2015. Characterization of strong and crystalline polyvinyl alcohol/montmorillonite films prepared by layer-by-layer deposition method. *International Journal of Polymer Science*, [online] Available at: <<http://dx.doi.org/10.1155/2015/123469>> [Accessed 20 August 2019].

Guo, W., Liu J., Zhang, P., Song, L., Wang, X. and Hu, Y., 2018. Multi-functional hydroxyapatite/polyvinyl alcohol composite aerogels with self-cleaning, superior fire resistance and low thermal conductivity. *Composites Science and Technology*, [e-journal] 158 (2018), pp.128–136. <https://doi.org/10.1016/j.compscitech.2018.01.020>.

Gutierrez, G., 2018. Oxydation of Clay Nanoreinforced Polyolefins. *Art Et Metiers*, 1(2010), pp.30-31.

Hajeeassa, K.S., Hussein, M.A., Anwar, Y. and Tashkandi, N., 2018. Nanocomposites containing polyvinyl alcohol and reinforced carbon-based nanofiller: A super effective biologically active material. *Nanobiomedicine*, 5 (2018), pp.1–12.

Henggu, K.U., Ibrahim, B. and Suptijah, P., 2019. Hydroxyapatite Production from Cuttlebone as Bone Scaffold Material Preparations. *Jurnal Pengolahan Hasil Perikanan Indonesia*, 22(1), p.1.

Jiang, X.C., Xia, C., Ye, D. and Liu, L., 2012. Properties of poly(vinyl alcohol) plasticized by magnesium chloride. *Gaodeng Xuexiao Huaxue Xuebao/Chemical Journal of Chinese Universities*, 33(8), pp.1872–1876.

- Jiang, X., Rui, Y. and Chen, G., 2009. The effect of polypropylene. *J Vinyl Addit. Technol*, 21(2), pp.129–133.
- Kamalbabu, P. and Mohan Kumar, G.C., 2014. Effects of Particle Size on Tensile Properties of Marine Coral Reinforced Polymer Composites. *Procedia Materials Science*, 5 (2014), pp.802–808.
- Kar, S., Kaur, T. and Thirugnanam, A., 2016. Microwave-assisted synthesis of porous chitosan-modified montmorillonite-hydroxyapatite composite scaffolds. *International Journal of Biological Macromolecules*, 82 (2016), pp.628–636.
- Lim, L.S., 2018. *Effects of Microwave Radiation on Properties of Polyvinyl Alcohol-Carbon Nanotube-Hydroxyapatite Blends*. BA. Universiti Tunku Abdul Rahman. Available at: <<http://eprints.utar.edu.my/id/eprint/3117>> [Accessed 20 August 2019].
- Ling, M.B., 2015. Investigation of Polyvinyl Alcohol (PVOH) Added Kenaf Nanowhisker And Montmorillonite (MMT). BA. Universiti Tunku Abdul Rahman. Available at: <<http://eprints.utar.edu.my/id/eprint/1601>> [Accessed 20 August 2019].
- Mohamed, A., Kahder, M., AlSaad, K. and AlMeer, S., 2013. Properties of nanoclay PVA composites materials. *A Qatar Foundation Academic Journal*, [e-journal], 2013 (1), pp. 1-9. <http://dx.doi.org/10.5339/connect.2013.1>.
- Mojtaba, K., Hamid, M., Mohammad Ali, S. and Mehdi, F., 2015. Nanoclay-reinforced electrospun chitosan/PVA nanocomposite nanofibers for biomedical applications. *RSC Advances*, 5(14), pp.10479–10487.
- Mostoufi, A., 2016. New applications of cuttlebone (CB) as a natural marine compound. *Jundishapur Journal of Natural Pharmaceutical Products*, 11(4), pp.10–11.
- Mourak, A., Hajjaji, M. and Alagui, A., 2019. Cured cuttlebone/chitosan-heated clay composites: Microstructural characterization and practical performances. *Journal of Building Engineering*, [e-journal] 2019(26), p.100872. <https://doi.org/10.1016/j.job.2019.100872>.
- Muhammad, A. and Zulfiqar Ali, R., 2018. Polyvinyl alcohol: A review of research status and use of polyvinyl alcohol based nanocomposites. *Polymer Engineering and Science*, 58(12), pp.2119–2132.
- Nur Fazreen, A., Hanafi, I. and Mohamad Kahar, W., 2017. Properties of polyvinyl alcohol/palm kernel shell powder biocomposites and their hybrid composites with halloysite nanotubes. *BioResources*, 12(4), pp.9103–9117.
- Ooi, K.Q., 2017. Study of Polyvinyl Alcohol-Montmorillonite Composites Enhanced by Carbon Nanotube. BA. Universiti Tunku Abdul Rahman. Available at: <<http://eprints.utar.edu.my/id/eprint/3255>> [Accessed 20 August 2019].

- Pan, Y. and Xiong, D., 2010. Preparation and characterization of nano-hydroxyapatite/polyvinyl alcohol gel composites. *Journal Wuhan University of Technology, Materials Science Edition*, 25(3), pp.474–478.
- Periasamy, K. and Kumar, G.C.M., 2019. TGA/DSC studies of marine coral reinforced polymer composites. *AIP Conference Proceedings*, [e-journal] 2057 (1), pp. 020033. <https://doi.org/10.1063/1.5085604>.
- Periasamy, K. and Mohankumar, G.C., 2016. Sea coral-derived cuttlebone reinforced epoxy composites: Characterization and tensile properties evaluation with mathematical models. *Journal of Composite Materials*, 50(6), pp.807–823.
- Poompradub, S., Ikeda, Y., Kokubo, Y. and Shiono, T., 2008. Cuttlebone as reinforcing filler for natural rubber. *European Polymer Journal*, 44(12), pp.4157–4164.
- Qiu, K. and Netravali, A.N., 2015. Polyvinyl alcohol based biodegradable polymer nanocomposites. *Biodegradable Polymers*, 1(13), pp.325–348.
- Rocha, J.H.G., Lemos, A.F., Agathopoulos, S., Valerio, P., Kannan, S., Oktar, F.N. and Ferreira, J.M.F., 2005. Scaffolds for bone restoration from cuttlefish. *Bone*, 37(6), pp.850–857.
- Sarin, P., Lee, S.J., Apostolov, Z.D. and Kriven, W.M., 2011. Porous biphasic calcium phosphate scaffolds from cuttlefish bone. *Journal of the American Ceramic Society*, 94(8), pp.2362–2370.
- Shang, S., Chiu, K.L., Yuen, M.C.W. and Jiang, S., 2014. The potential of cuttlebone as reinforced filler of polyurethane. *Composites Science and Technology*, [e-journal] 93 (2014), pp.17–22. <http://dx.doi.org/10.1016/j.compscitech.2013.12.019>.
- Sinha, A., Das G., Kumar Sharma, B., Prabahan Roy, R., Kumar Pramanick, A. and Nayar, S., 2007. Poly(vinyl alcohol)-hydroxyapatite biomimetic scaffold for tissue regeneration. *Materials Science and Engineering C*, 27(1), pp.70–74.
- Soltani, Z. , Ziaie, F., Ghaffari, M., Afarideh, H. and Ehsani, M., 2013. Mechanical and thermal properties and morphological studies of 10MeV electron beam irradiated LDPE/hydroxyapatite nano-composite. *Radiation Physics and Chemistry*, [e-journal] 83 (2012), pp.79–85. <http://dx.doi.org/10.1016/j.radphyschem.2012.10.012>.
- Soundararajah, Q.Y., Karunaratne, B.S.B. and Rajapakse, R.M.G., 2010. Mechanical properties of poly(vinyl alcohol) montmorillonite nanocomposites. *Journal of Composite Materials*, 44(3), pp.303–311.

Tee, T.T., Lee, T.S., Gobinath R., Bee, S.T., David Hui, Rahmat, A.R., Kong, I. and Fang, Q., 2013. Investigation of nano-size montmorillonite on enhancing polyvinyl alcohol-starch blends prepared via solution cast approach. *Composites Part B: Engineering*, [e-journal] 47 (2013), pp.238–247. <http://dx.doi.org/10.1016/j.compositesb.2012.10.033>.

Thakur, G., Singh, A. and Singh, I., 2016. Chitosan-montmorillonite polymer composites: Formulation and evaluation of sustained release tablets of aceclofenac. *Scientia Pharmaceutica*, 84(4), pp.603–617.

Uma Maheshwari, S., Samuel, V.K. and Nagiah, N., 2014. Fabrication and evaluation of (PVA/HAp/PCL) bilayer composites as potential scaffolds for bone tissue regeneration application. *Ceramics International*, [e-journal] 40(6), pp.8469–8477. <http://dx.doi.org/10.1016/j.ceramint.2014.01.058>.

Wang, S.F., Shen, L., Tong, Y.J., Chen, L., Phang, I.Y., Lim, P.Q. and Liu, T.X., 2005. Biopolymer chitosan/montmorillonite nanocomposites: Preparation and characterization. *Polymer Degradation and Stability*, 90(1), pp.123–131.

Wei, W., Song, W. and Zhang, S., 2014. Preparation and characterization of hydroxyapatite-poly(vinyl alcohol) composites reinforced with cellulose nanocrystals. *BioResources*, 9(4), pp.6087–6099.

Xue, K., Teng, S.H., Niu, N. and Wang, P., 2018. Biomimetic synthesis of novel polyvinyl alcohol/hydroxyapatite composite microspheres for biomedical applications. *Materials Research Express*, 5(11), pp.115401.

Yasmin and Kalyani, D., 2015. Naturally Derived Porous Hydroxyapatite/Polymer Biocomposite of Cuttlebone and Eggshell for Dental and Orthopedic Applications. *International Journal for Research in Applied Science and Engineering Technology*, 3(VI), pp.471–478.

Zanela, J., Bilck, A.P., Casagrande, M., Grossmann, M.V.E. and Yamashita, F., 2018. Polyvinyl alcohol (PVA) molecular weight and extrusion temperature in starch/PVA biodegradable sheets. *Polímeros*, 28(3), pp.256–265.